JULY, 2014

ELECTROSTATIC POTENTIAL IN SOLIDS

DANIEL MENÉNDEZ CRESPO

MASTER THESIS. EUROPEAN MASTER EMTCCM.

Quantum Chemistry Group.
Departamento de Química Física y Analítica.
Área de Química Física.
Universidad de Oviedo.

JULIO, 2014

POTENCIAL ELECTROSTÁTICO EN SÓLIDOS

DANIEL MENÉNDEZ CRESPO

TESIS DE MÁSTER. MÁSTER EUROPEO EMTCCM.

Grupo de Química Cuántica.
Departamento de Química Física y Analítica.
Área de Química Física.
Universidad de Oviedo.

D. Ángel Martín Pendás, Catedrático del Departamento de Química Física y Analítica de la Universidad de Oviedo y Coordinador del Máster Europeo en Química Teórica y Modelización Computacional,

CERTIFICA:

Que el trabajo titulado **Electrostatic Potential in solids**, ha sido realizado por D. Daniel Menéndez Crespo, bajo la tutela del profesor titular Víctor Luaña Cabal con el fin de optar al título que otorga el Máster en Química Teórica y Modelización Computacional.

Oviedo, 24 de Julio de 2014.

Fdo.: Ángel Martín Pendás.
Coordinador del Máster Europeo en Química Teórica y Modelización Computacional

D. Víctor Luaña Cabal, Profesor Titular de Química Física del Departamento de Química Física y Analítica de la Universidad de Oviedo,

CERTIFICA:

Que el trabajo titulado **Electrostatic Potential in solids**, ha sido realizado bajo su dirección por D. Daniel Menéndez Crespo, constituyendo su Tesis de Máster, cuya presentación autoriza.

Oviedo, 24 de Julio de 2014.

Fdo.: Víctor Luaña Cabal.

AGRADECIMIENTOS

Primero y ante todo quiero agradecer a mi familia y amigos su apoyo. A Víctor quiero agradecerle su paciencia, su increíble dedicación en las clases, su tiempo dedicado a supervisar mi trabajo y un sinfín de cosas más. Muchas gracias.

A Aurora por su ayuda continuada con tareas administrativas, incluso cuando otras tareas más importantes la requieren, y por preocuparse por mí.

A Aurora, Víctor, Ángel y Enrique por ofrecerme la posibilidad de realizar una estancia en Nancy.

A los profesores del Grupo de Oviedo por mostrame el fascinante campo de la química cuántica y ofrecerme sus consejos. A los profesores del máster por hacer posible la supervivencia de un máster con tan amplio abanico de conocimientos.

A Enrique por sus entretenidas y clarificantes charlas sobre temas científicos durante nuestras frecuentes sobremesas. Gracias por responder a mis incesantes pregunatas. Mi estancia en Nancy ha sido muy agradable gracias a tí. Guardo muy buenos recuerdos de compañeros del grupo: Benoît Guillot, Christian Jelsch y Pierrick Durand así como de mis compañeros de despacho Amine y Wilba especialmente.

A Alberto por su atención a los problemas que han aparecido a lo largo del proceso y su inestimable ayuda. Igualmente, Ignasi me ha proporcionado información relevante para poder seguir adelante.

A mis compañeros: Mamel, Miriam, David, Marcos, Alfonso, Roberto, Marian, Hussein por hacer del laboratorio un entorno agradable. Y Fernando en particular como compañero desde la licenciatura además de amigo.

Los cursos intensivos han sido menos duros con la compañia de mis colegas de máster. Siempre es un placer reencontrarse y compartir experiencias.

Gracias a todos.

ABSTRACT

The organic conductor BTDMTTF–TCNQ ($C_{10}H_8S_6^+ \cdot C_{12}H_4N_4^-$) is a charge-transfer complex that behaves as an almost pure 1D metal, showing metallic character down to 26 K [33]. The magnitude of the intermolecular charge transfer at T = 130 K was initially estimated at approximately 0.7 e from the values of the multipolar parameters obtained in an experimental charge density study [8]. Recently, a QTAIM analysis [3] applied to the same multipolar charge density model revealed more accurate atomic charges. Indeed, while charges inferred from multipoles replicate integrated charges for coarse grained atomic groups, they fail when fine granularity (e.g. C, N) is demanded. In addition, contributions to charge transfer are spread amongst several atoms instead of being localized in sulfur atoms, as previously pointed out [8]. Also, we have systematically identified the interactions present in the crystal phase using the topology of the electrostatic potential [21, 22] and the Laplacian of the electron density with the `MoPro` [15] and `critic2` [26, 28] programs.

RESUMEN

El conductor orgánico BTDMTTF–TCNQ ($C_{10}H_8S_6^+ \cdot C_{12}H_4N_4^-$) es un complejo de transferencia de carga que se comporta como un metal quasi-monodimensional hasta una temperatura de 26 K [33]. La magnitud de la trasferencia de carga intermolecular ha sido inicialmente estimada a T = 130 K como aproximadamente 0.7 e a partir de los valores de los parámetros multipolares obtenidos en un estudio de la densidad de carga electrónica previo [8]. Recientemente, la aplicación de un análisis QTAIM al mismo modelo multipolar ha revelado unos valores de cargas atómicas más precisos. De hecho, mientras las cargas inferidas con los multipolos replican las cargas integradas para grupos atómicos, estos fallan cuando se requieren los valores de cargas atómicas individuales. Además, las contribuciones atómicas a la transferencia de carga no están localicadas en un grupo reducido como se predijo con anterioridad [8], sino que existen varios contribuyentes y su peso exacto es desconocido. También hemos identificado sistemáticamente las interacciones presentes in la fase cristalina usando la topología del potencial electrostático [21, 22] y de la Laplaciana de la densidad electrónica con los programas `MoPro` [15] y `critic2` [26, 28].

ACRONYMS

AIM	Atoms In Molecules theory
BCP	Bond Critical Point or $(3,-1)$ ρ-**CP**
BTDMTTF	bis(thiodimethylene)–tetrathiafulvalene
CCD	Charge-Coupled Device
CP	Critic Point
CUBE	`Gaussian` parallepiped grid 3D data file
`critic2`	A program for the topological anaylisis of real-space scalar fields in periodic systems
CWM	Constrained Wavefunction Method
DFT	Density Functional Theory
EBCP	Electrostatic Bond Critical Point or $(3,-1)$ ϕ-**CP**
ED	Electronic Density (one body electron density)
ELF	Electron Localization function
ELI	Electron Localizability Indicator
EOS	Equation Of State
ESP	Electrostatic Potential (one body electrostatic potential)
`espresso`	opEn Source Package for Research in Electronic Structure, Simulation, and Optimization
`Gaussian`	Electronic structure code
HF	Hartree Fock Optimization of a multielectronic system monoelectronic orbitals through minimization of a Russell-Saunders state energy under spin-orbitals orthonormalization condition.
HK	Hohenberg–Kohn theorems
IAM	Independent Atom Model
IAS	Inter Attractor Surface
IUCR	International Union of Crystallography
KS	Kohn–Sham equations

LSEXP Multipolar refinement program by Hirshfeld

LATITUDINAL Latitudinal pseudo-isolated dimer

LHS left–hand side

LONGITUDINAL Longitudinal pseudo-isolated dimer

MEM Maximum Entropy Method

MEP Molecular Electrostatic Potential

MOLLY Multipolar refinement program by Hansen and Coppens

MoPro Cristallographic least square refinement package allowing structural or charge density studies of cristal stuctures of variable sizes, ranging from small molecules to biological macromolecules.

MoProViewer A graphical interface to MoPro

NCI Non Covalent Interactions

Orca Electronic structure code

POP Multipolar refinement program by Craven, Weber, He

QE Quantum espresso equations

Plane waves + pseudopotentials. Electronic structure code for extended systems.

QCT Quantum Chemical Topology

QTAIM Quantum Theory of Atoms in Molecules

RDG Reduced Density Gradient

RHS right–hand side

RDM Reduced Density Matrix

TTF tetrathiafulvalene

TCNQ 7,7,8,8–tetracyanoquinodimethane

UNESCO United Nations Educational, Scientific and Cultural Organization

UPF Unified Pseudopotential File

Pseudopotential standard file format.

VSCC Valence Shell Charge Concentration

VSCD Valence Shell Charge Depletion

VSEPR	Valence Shell Electron Pairs Repulsion
VMoPro	Scalar fields analysis tool
XDM	Exchange Dipole Moment
XRD	X–Ray Diffraction

CONTENTS

INTRODUCTION

The nature of chemical bonding remains one the most important unanswered questions in chemistry, joining an interdisciplinary community that tries to disentangle the reasons leading to bonding formation/breaking and their prediction to build new materials, understand biochemical processes, control material properties. Much of the technological advances are guided by new and improved knowledge of the nanostructure of matter and its implication at the macroscopic level.

The ability to analyze experimental and theoretical densities with a quantum mechanically grounded theory has led to a great progress of charge density analysis during the last decades. Books [11, 23, 35, 36] and references therein show an overview of the last decade. The density is a fundamental variable of nature as stated through the first Hohenberg–Kohn (HK) theorem. It is the *lingua franca* of X–Ray Diffraction (XRD) , Density Functional Theory (DFT) and Quantum Theory of Atoms in Molecules (QTAIM).

However, the situation is far from desired. The information interchanged is limited to the one-particle density. Though the topological partition of the electronic density provides descriptors soon identifiable from chemical intuition, their meaning isn't still fully known and the information retrieved isn't complete enough to fully describe the bonding nature. For example, bond orders are highly dependent on the correlation. Therefore new descriptors not coming from the density but from the Reduced Density Matrices (n–RDM) are used instead to complement the results of QTAIM. The understanding of their nature becomes a task of prime importance.

Among the many Quantum Chemical Topology (QCT) descriptors already present, aside from the well studied density, the electrostatic potential is the easier target to look at as a new source of chemical information.

There are many works published about the electrostatic potential but only a few analyze the topology in molecules, and even fewer in solids [21, 22, 39]. We considered appropriate the use of the electrostatic potential to study an organic conductor in crystal phase with the aim of extending the previous work by Mata et al.

The structure of this master thesis is the following: Chapter 1 reviews the main concepts of experimental charge density analysis. QTAIM topological analysis is summarized in Chapter 2. Chapter 3 focuses on the electrostatic potential and its topology. Chapter 4 contains the results of our work applying topological approaches to the BTDMTTF–TCNQ crystal.

Atomic units are used except where otherwise is indicated.

INTRODUCCIÓN

La naturaleza del enlace químico es hoy en día uno de los problemas fundamentales de la química que sigue sin comprenderse completamente. Su estudio une una gran comunidad Ãnter disciplinaria con el objetivo común de descifrar las claves que rigen la formación/rotura de enlace, su predicción para fabricar nuevos materiales, entender procesos bioquímicos o controlar las propiedades de un material. Muchos de los avances tecnológicos recientes han sido guiados por un conocimiento nuevo o más profundo sobre la nanoestructura de la materia y su implicación a nivel macroscópico.

La posibilidad de analizar densidades electrónicas experimentales y teóricas con una teoría fundada en principios mecano-cuánticos ha dado lugar a un gran progreso en el análisis de densidad de carga durante las últimas décadas. Los libros [11, 23, 35, 36] y las referencias contenidas en ellos son una prueba de ello. La densidad electrónica es una variable fundamental de la naturaleza tal y como afirma el teorema de Hohenberg–Kohn (HK). Es la *lingua franca* de Diffracción de Rayos-X (XRD), Teoría del Funcional de Densidad (DFT) y Teoría Quántica de Átomos en Moléculas (QTAIM).

De todas formas, la situación dista de ser la deseada. La información intercambiada se limita a la densidad mono-electrónica. Aunque la partición topológica de la densidad electrónica provee descriptores que son fácilmente identificables con conceptos químicos tradicionales, su significado no es comprendido en todo detalle y la información obtenida no es suficientemente completa como para describir el enlace químico. Por lo tanto, se necesitan nuevos descriptores que provengan no de la densidad mono-electrónica, sino de las Matrices de Densidad Reducida (n–RDM) para complementar los resultados de QTAIM. Entender su naturaleza es una tarea de importancia crucial.

Entre los muchos descriptores de la Topología Químico Cuántica (QCT), aparte de la bien estudiada densidad electrónica, el potencial electrostático es el objetivo más fácil en el que fijarse como una nueva fuente de información química.

Hay muchos trabajos sobre el potencial electrostático, pero sólo unos pocos tratan la topología en moléculas, y aún menos en sólidos [21, 22, 39]. Hemos considerado oportuno aplicar el potencial electrostático en el estudio de un conductor orgánico en fase cristalina con el fin de continuar extendiendo los trabajos previos de Mata et al.

La estructura de esta tesis de máster es la siguiente: En el Capítulo 1 se revisan los principales conceptos en análisis experimental de carga electrónica. El análisis topológico QTAIM se resume en el

Capítulo 2. El Capítulo 3 se centra en el potencial electrostático y su topología. El Capítulo 4 contiene los resultados de nuestro trabajo aplicando la topología del potencial electróstatico al cristal BTDMTTF–TCNQ.

Se utilizan unidades atómicas, excepto cuando lo contrario sea indicado.

Part I

Methodology

1 CRYSTALLOGRAPHY

CONTENTS

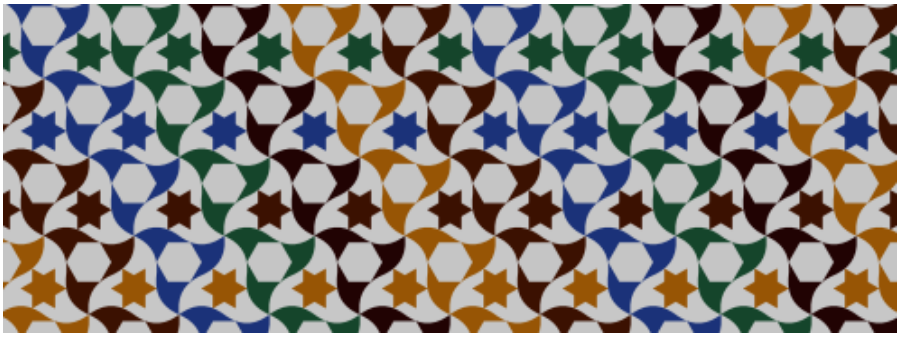

Symmetry is not only a mathematical abstraction, it is useful to simplify lots of physical problems and artists have found in it a source of beauty. Many Alhambra mosaics, such as the one above, belong to any of the wallpaper symmetry groups.

1.1 INTRODUCTION

The IUCR and UNESCO agreed to declare 2014 as the International Year of Crystallography to commemorate the centenary of Max von Laue's Nobel Prize in Physics. The goal is to promote the knowledge of this influential discipline. This master thesis is just one example that shows the close relation of quantum chemistry and crystallography.

It was Kepler, 400 years ago, who first observed that symmetry underlies the disposition of atoms or molecules in condensed matter while inspecting snowflake patterns. We know today that symmetry is present everywhere. Many solids in nature are periodic arrangements of atoms presenting a type of space group symmetry [12]. The whole crystal can be regenerated from a parallepiped fraction of the crystal, unit cell, just by applying translations parallel to the edges. This simplifies a lot their study.

The most valuable experimental technique for the determination of the 3D structure of crystalline samples is XRD. It is of utmost importance to allow the discovery of new materials for the next technological era, drugs to treat human diseases or investigate minerals underpinning the geology of Earth. Nowadays X-ray crystallography is recognized as an essential tool.

1.2 DIFFRACTION

X-rays allow us to "see" the atoms. The choice of this particular radiation is based on the similitude of their wavelength to interatomic spacings. The usefulness of X-ray techniques relies on a proper description of rays-matter interactions. When a X-ray beam strikes a crystal, the beam is absorbed or scattered from the crystal. Atomic nuclei are thousands of times smaller than the diameter of the atoms and they mostly do not participate in the scattering process. Scattered photons may or may not undergo an energy transfer, both are termed inelastic and elastic scattering respectively. If the wavelength of the incident beam and the lattice spacing are comparable constructive interference occurs. The process is called diffraction.

The path difference is conditioned by atomic spacings and the orientation of the beam. W. H. Bragg and his son used a simple model of atoms contained in equally spaced planes and found a law,

$$\lambda = 2d \sin \theta, \tag{1}$$

that rules the conditions needed to be satisfied for diffraction to happen. The wavelength of the beam (λ) must equal twice the interplanar distance (d) multiplied by the sine of the incident beam angle (θ). The same law works as well for neutron or electron diffraction.

1.3 ELASTIC X–RAY DIFFRACTION

There are two main techniques associated to X–Ray Diffraction. One is single crystal diffraction and the other is powder diffraction. A powder difractogram has not enough peaks to correctly determine the huge number of density modeling parameters. Our data has been gathered with the first technique.

The orientation of scattered X-Ray beams is defined by the scattering vector $\mathbf{H}$. Scattered peaks are collected by a bidimensional CCD detector. The amplitude, $A(\mathbf{H})$, of the diffraction peaks is proportional to the Fourier transform of the thermally averaged electron density, $\rho^{dyn}(\mathbf{r})$, in the unit cell:

$$I(\mathbf{H}) = |A(\mathbf{H})|^2 \approx |F(\mathbf{H})|^2 = \left| \int_V \rho^{dyn}(\mathbf{r}) e^{2\pi i \mathbf{H}\cdot\mathbf{r}} \, d\mathbf{r} \right|^2 . \tag{2}$$

The first step towards achieving a high quality density description is obtaining a good crystal. Another less relevant factor is the type of crystal (ionic crystals usually diffract better than molecular ones with the same quality, because they have tightly bounded electrons) and mosaicity.

Obviously we cannot realize an infinite number of measurements. The limit

$$|\mathbf{H}|_{max} = \frac{2 \sin \theta_{max}}{\lambda} \tag{3}$$

is set by the type of radiation used and the geometry of diffractometers. The signal is each time weaker as we augment the incidence angle. As a result, we have to truncate the Fourier sum. A huge number of peaks need to be measured to complete the Fourier sum as much as possible. Radiations with small wavelengths increase the number of measurable peaks but the intensity is inversely proportional to the wavelength, so the expected improvement is canceled. The decreasing ratio of amplitudes is emphasized with the temperature.

The main problem comes here. The structure factors are complex numbers of which we only have information about its complex product, $|\mathbf{F}|^2$. The phase has been lost during the experiment and we need to recover it anyway to solve the structure and density properly. The relevance of the phase information is crucial because most of the information is coded in the phase.

Once the diffraction peaks are obtained, absorption and other experimental effects introduced in the intensities are corrected.

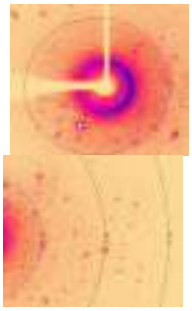

1.4 DENSITY MODELING

The unit cell dynamical density can be formally decomposed in pseudo-atomic densities and Dirac's deltas at average atomic positions. The dual of pseudo atomic densities are atomic form factors.

Atomic form factors include the Debye–Waller factor, that measures the average thermal motion. Atomic form factors are diminished with increasing Bragg angles. Even at very low temperatures. Heavy atoms have a longer tail, although the maximum angle achieved is barely increased.

Thermal factors are deconvoluted from the static density using an harmonic model of nuclei motion. Low temperature is needed to decrease nuclei motion. Thus the harmonic approximation becomes a better model and the deconvolution of thermal factors from static density fitting parameters is improved. The static density has relativistic, matrix and correlation effects included, and does not correspond to the ground state. The static density is described by a superposition of pseudo-atomic densities

$$\rho(\mathbf{r}) = \sum_{i=1}^{N_{at}} \rho_{at}(\mathbf{r}). \tag{4}$$

There are three models to refine the density with different levels of sophistication: A naïve approach, the IAM model, is to consider spherical atomic densities. This approximation is good for core electrons. The difficult part to model is the valence density. The aim of other models is to recover the anisotropy of the valence density. In our next approximation, the density is allowed to contract or to expand, that is the *kappa* model. If we go further, we can allow the density to be non spherical adding multipolar expansions, the multipolar model.

The Maximum Entropy Method (MEM) is an alternative to the multipolar model to refine charge densities. It treats directly the dynamical density. The dynamical density obtained can be used [25] to apply QTAIM analysis but we should remember that it is not the same as the static density.

The static density is refined following a least-squares minimization of

$$M = w_{\mathbf{H}} \left(F_{obs}(\mathbf{H})^2 - F_{theo}(\mathbf{H})^2 \right)^2 \tag{5}$$

the difference between observed and calculated intensities, each one has a weight $w_{\mathbf{H}}$.

1.4.1 Independent Atom Model (IAM)

Under the isolated spherical approximation (IAM) the density of each atom is build up from the radial part of *ab initio* wave functions . Therefore, the atomic scattering factors are known from Hartree–Fock calculations of ground state free atoms. Even though this model is simplistic it works well for heavy atoms owing to the small proportion of valence shell electrons against total density. For hydrogen

atoms the approximation is not good enough even to describe properly atomic coordinates. They have only one electron and their contribution is usually too small. IAM overestimates their bonding because the unique electron that it has is displaced towards the bond and therefore the centroid that determines the atomic position is shifted in the same direction. The problem remains even with better models.When the system has hydrogen atoms, the X-ray parameters refinement has to be complemented with neutron diffraction data.

Only thermal parameters and atomic coordinates are refined within this model.

The envelope of core electron form factors do not decrease much with Bragg's angle incrementation. The easiness of the IAM model suggests to perform first a refinement with high angle data and then proceed with low angle data to refine the valence shell charge. The problem of this *high order refinement* is that the intensity of peaks is very small.

1.4.2 Kappa formalism

Two new parameters have to be refined in the *kappa* model. The κ parameter allows the density to contract or expand scaling the radial function. $\kappa^3\rho_{val}(\kappa r)$ is normalized to be a one electron density.

$$\rho_{at}(\mathbf{r}) = \rho_{core}(r) + P_{val}\kappa^3\rho_{val}(\kappa r) \tag{6}$$

P_{val} is the valence shell population parameter. It contains information to analyze charge transfer.

The density is spherically symmetric.

1.4.3 Multipolar pseudo-atom model

The kappa model does not recover angular anisotropy at all. Atoms in a crystal are surrounded by others that disturb the electronic density of its neighbors. Some directions are preferred for interatomic interaction. Nearest neighbors of different electronegativity induce charge transfer and dipole moments appear. Non spherical orbitals produce the same effect. Is there any function that fills the gap between the theoretical and experimental densities $\Delta\rho(r) = \rho(r) - \rho_0(r)$? The framework [37] to generalize the atomic scattering factors was set by Stewart, after some previous work with multipolar functions. Years later Hansen and Coppens developed the definitive model to extract accurate electronic densities [7, 13]. There are three implementations with similar characteristics: `MOLLY`, `LSEXP` and `POP`.

The pseudo-atomic multipolar density is

$$\rho_{at}(\mathbf{r}) = \rho_{core}(r) + P_{val}\kappa^3\rho_{val}(\kappa r) + \sum_{l=0}^{l_{max}} \sum_{m=-l}^{m=l} \kappa'^3 R_{nl}(\kappa' r) P_{lm} Y_l^m(\theta, \phi). \tag{7}$$

It is a fuzzy atomic partitioning

The first two terms are the same found in the *kappa* model. They contain all the charge of the pseudo-atoms. The last term is a multipolar expansion that interchanges charges between the lobes of real spherical harmonic functions $Y_l^m(\theta, \phi)$.

The density fitting is very sensitive to the choice of optimal radial function, $R_{nl}(\kappa' r)$. The monopole P_{00} is usually zero to simplify physical interpretation.

Typical is the case of $l_{max} = 1$ for hydrogens, $l_{max} = 3$ for the second row elements in the periodic table, and $l_{max} = 4$ for the rest. The model cannot be extended to heavy elements because the valence shell is very thin and high angular orbitals delocalize the charge making it nearly spherical, so high order multipoles are needed to describe correctly the density. Thus, the physical interpretation of multipolar terms becomes difficult. The model reaches its limits. κ' is analogous to κ.

The ratio parameters to fit over data available is too high. Using the multipolar model 27 or 36 parameters have to be fitted for each non hydrogen atom. *High order refinement* is necessary to avoid correlation of thermal factors and multipolar parameters. They recover different types of anisotropy.

The great benefit of this model is that phases are also improved.

The expansion given by the multipolar model for the density is analogous to the expansion by the LCAO formalism, but all terms are atom-centered. The multipolar model has limitations to describe diffuse electronic distributions, $\rho(\mathbf{r}) \approx 0$, such as interatomic regions, due to the nucleus-centered nature mentioned above.

Remember that the density resulting from the LCAO formalism expands the wave function in one and two center terms.

Parameters of appendix A were refined with `MOLLY` and evaluated with the `MoPro` [15] package.

1.4.4 Density maps

Deformation maps, $\Delta\rho(r) = \rho(r) - \rho_0(r)$, reveal redistributions of the electron density with respect to spherical non interacting isolated atoms, mapped on a suitable molecular plane. Density arrangements appear at bonds, lone pairs. For a long time density maps were the main source of chemical information [7], but now they have been replaced by QTAIM analysis. Nevertheless, density maps are a good assessment tool to decide the quality of the refinement.

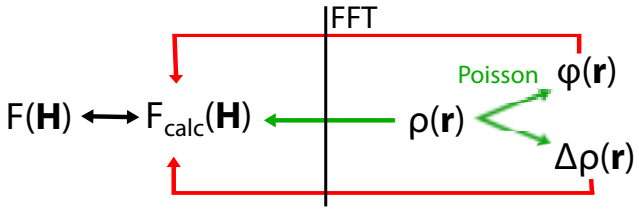

Figure 1: F(H) are the experimental structure factors. The experimental density is the one that best regenerates the experimental structure factors. Both are related by a Fourier transform. The Laplacian is obtained with numerical derivation of the density, and the electrostatic potential by Poisson law.

1.5 OTHER EXPERIMENTAL OBSERVABLES

The electrostatic potential, electric field, electron density, electron density gradient, and Laplacian of the electron density may be obtained through their corresponding Fourier transformation of the structure factors. They also depend on $|\mathbf{H}|^{-2}$, $|\mathbf{H}|^{-1}$, $|\mathbf{H}|^{0}$, $|\mathbf{H}|$, and $|\mathbf{H}|^{2}$ respectively. The completeness of the Fourier series is critical for the density gradient and Laplacian.

Otherwise, we obtain the electrostatic potential from the multipolar model density.

$$\phi(\mathbf{r}) = \frac{1}{V}\sum_{\mathbf{H}} \frac{F(\mathbf{H})}{\mathbf{H}^2} e^{-2\pi i \mathbf{H}\mathbf{r}} \tag{8}$$

The Poisson equation links the density and the electrostatic potential. The electrostatic potential reference is now arbitrary. Absolute values are not so important, relative values are what we are interested in. The topology is about critical points, that is, points with a local field value greater than the proximate points. The zero potential can be obtained from electron diffraction. But for a molecular crystal it is not possible because the sample would be destroyed. It is only feasible for ionic crystals. Electron beams interact more strongly with matter than X-rays. So, we no longer talk about the electrostatic potential of the solid, instead we take a moiety of the crystal and from the multipolar parameters associated to the atoms in the moiety we obtain the electrostatic potential. The expression is similar to the multipolar expansion and the evaluation is analytic. We are analyzing pseudo-isolated molecules, however, the parameters are those of the crystal.

Pseudo-isolated analysis is a common crystallographic procedure to focus on the interactions in specific parts of the crystal

The Laplacian is evaluated with numerical differentiation of the multipolar density.

$$\nabla^2\rho(\mathbf{r}) = \frac{1}{V}\sum_{\mathbf{H}} \mathbf{H}^2 F(\mathbf{H}) e^{-2\pi i \mathbf{H}\mathbf{r}} \tag{9}$$

2 QUANTUM CHEMICAL TOPOLOGY

CONTENTS

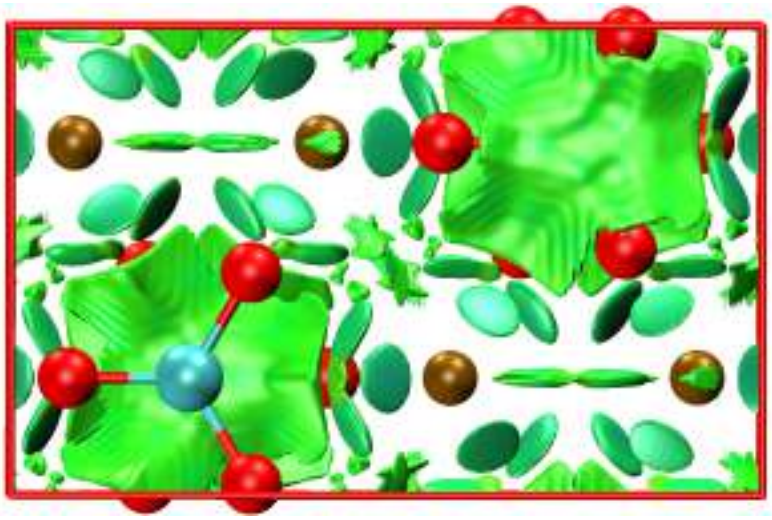

Reduced Density Gradient (RDG) isosurfaces of Aragonite at equilibrium geometry. The colouring corresponds to a blue-green-red scale of $\text{sign}(\lambda_2)\rho$ ranging from -0.05 to 0.05 a.u. values.

2.1 A QUANTUM BONDING THEORY

> If, in some cataclysm, all of scientific knowledge were to be destroyed, and only one sentence passed on to the next generations of creatures, what statement would contain the most information in the fewest words? I believe it is the atomic hypothesis that all things are made of atoms. In that one sentence, you will see, there is an enormous amount of information about the world, if just a little imagination and thinking are applied.
>
> R. P. Feynman

The Quantum Theory of Atoms in Molecules (QTAIM) [3] appeared during the 60s as a new theory with the aim to describe chemical bonding using the electron density. Berlin established [5] a real space partition of diatomic molecules in binding and non-binding regions attending to the electrostatic forces using the Hellman–Feynman theorem. Bader payed attention to the derivatives of the density an he realized that the space could be divided by zero derivative surfaces. The extension of this concept to polyatomic molecules and the later realization that they correspond to atomic regions are the foundations of AIM. At the beginning it was far from trivial how to describe the quantum mechanics of atoms in molecules, that is, open systems. Is there a way to define all the quantum observables of an atomic system belonging to a molecular system? A key pre-requisite is to define the quantum action integral, kindly provided by Schwinger [4]. Swinger's action principle requires smooth and continuous conditions. As a result, the topological and quantum descriptions of an atom are the same. Besides the concept of chemical groups is also recovered and the transferability of atomic properties between similar groups can be examined.

The ever increasing number of papers published that make use of QTAIM support its undeniable success as a theory of bonding, being the crystallography community one of its earlier adopters. The parallel use of the multipolar model and QTAIM boosted the charge density analysis during the last years. For the time being, novel extensions of QTAIM appeared [30], they require more information than the diagonal electron density matrix and their use is still restricted to a full electron *ab initio* calculation, except for a rather new approach proposed by Jayatilaka. The Constrained Wavefunction Method (CWM) performs at the same time the energy minimization iterations and the density refinement trying to get the best result. With that approach the density is represented by a Slater determinant. Henceforth, we have off-diagonal 1–RDM elements. The CWM is a good promise but only a few examples were performed yet.

The four main steps of a topological analysis are as follows: a) localize all critical points of the scalar field b) classify the critical

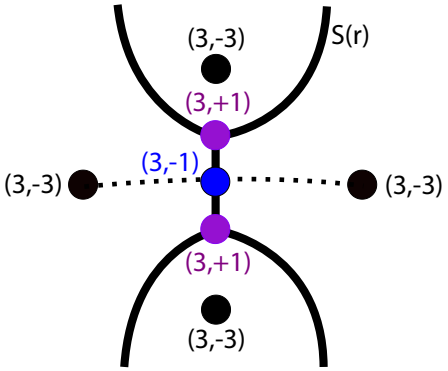

Figure 2: Most frequent critical points found in the electron density and the limits of atomic basins.

points examining the Laplacian of the field c) obtain the basins, d) and integrate properties over the basins. R. F. Bader and his group demonstrated the importance of this recipe by studying exhaustively the electron density. Many extensions (ESP, NCI, Ehrenfest force field, ELF, ELI, second order density, Laplacian of the density) of the topological analysis have been investigated or are in progress and the global theory is suggested to be called Quantum Chemical Topology (QCT). The source of QCT descriptors are 1- and 2-RDMs.

LAPLACIAN OF THE ELECTRON DENSITY [31] Related to local charge concentration and depletion. Recovers the VSEPR model.

ELECTROSTATIC POTENTIAL [21, 22] Electrostatically shielded regions and influence zones.

ELECTRON LOCALIZATION FUNCTION [2] Localizes core and valence pair regions such as covalent bonds or lone pairs.

NON COVALENT INTERACTIONS [16] Regions of low density that represent and characterize van der Waals interactions, hydrogen bonds, and steric repulsion.

EHRENFEST FORCE FIELD [14] The electrostatic force felt by an electron in a molecule due to the presence of all the other electrons and nuclei in the system.

MAXIMUM PROBABILITY DOMAINS [32] Probability of finding regions of space with an exact number of electrons.

NATURAL ADAPTATIVE ORBITALS [9] Decompose multicenter bonding indices in one center components allowing the analysis of correlated and non-correlated wavefunctions on the same basis.

Several research groups around the world are currently researching in the theory born from Bader's work.

2.2 TOPOLOGY INDUCED BY A VECTOR FIELD

The Ehrenfest force field is a vector field itself and the dynamical system has physical meaning

In most cases descriptors are scalar fields. Thus implies that the topology is performed via their associated gradient fields. Those fields are characterized by so-called critical points, i.e. points with vanishing first derivatives ($\boldsymbol{\nabla}\rho(\mathbf{r}) = \mathbf{0}$). Seen from another point of view, it is an *hypothetic* dynamical system with stationary points.

There are several types of critical points, the way to distinguish them is using the Laplacian. The procedure is the same for any field, but the physical interpretation varies. The density will be our guiding example. At a point of $\mathbb{R}^3$ space the electron density Laplacian is,

$$\nabla^2\rho = \frac{\partial^2\rho}{\partial x'^2} + \frac{\partial^2\rho}{\partial y'^2} + \frac{\partial^2\rho}{\partial z'^2} = \mathrm{Tr}(\mathrm{diag}(\mathbb{H}_\rho)) = \sum_{i=1}^{3}\lambda_i, \tag{10}$$

the sum of diagonal components resulting from the diagonalization of the Hessian ($\mathbb{H}_\rho$) in principal curvatures (λ_i).

Critical points are characterized by the rank of the Hessian (r) and signature ($s = \sum_i {}^{\lambda_i}/_{|\lambda_i|}$), commonly abbreviated as (r, s). A critical point with one or more Hessian eigenvalues equal to zero is called a degenerate critical point. Degenerate density critical points appear at instable configurations. There are four types of non-degenerate density critical points:

- Nuclear critical points $(3, -3)$: A maximum in the three main axes. They are almost always located at nuclei positions.
- Bond critical points $(3, -1)$: they are located in a minimum between two nuclei. The density is a maximum in the other two directions. They are located at the border of two basins. The set of points connecting it with other nuclear points following the maximum gradient define what has been called *bond paths*.
- Ring critical points $(3, +1)$: They appear in the center of aromatic rings.
- Cage critical points $(3, +3)$: A minimum in the tree main axes.

Bond critical points are the most interesting ones. The properties at them can be correlated with chemical behavior. The density value is related to the strength of covalent bonds. The Laplacian values are related to the strength of non-covalent (closed shell) interactions. Only equivalent bond pairs can be compared. The ellipticity is often used as an indicator of π character for an interaction. The ellipticity, using $\lambda_1 < \lambda_2 < \lambda_3$, of a bond critical point is defined as

$$\epsilon = \frac{\lambda_1}{\lambda_2} - 1. \tag{11}$$

It gives a measure of the electron distribution anisotropy in the principal axes perpendicular to the bond path. For σ and triple bonds cylindrical symmetry is presented and the ellipticity value is ≈ 0, for π interactions electron concentrates preferentially in one of the planes which give a maximum for the charge at the critical point, so its value is $\neq 0$.

The topology of any scalar field is determined by its critical points and asymptotic behaviour at an infinite sphere, the mathematical relation is contained in the Hopf-Poincaré relationship. In molecules the relationship of the electron density is

$$n - b + r - c = 1, \tag{12}$$

where n, b, r and c denote the number of nuclear, bond, ring and cage critical points. In periodic systems the asymptotic behaviour is different, the relation equals 0.

The content of this section could be called chemical topography. The following section describes how to assign physical properties to chemical entities using the topology of the field.

2.3 THE ATOMIC PARTITIONING OF MOLECULAR PROPERTIES

Topological methods aim at the segmentation of a vector field into real space areas of different flow behavior. All vector lines end either at an attractor (nuclear critical point) or at a saddle point. The spatial region given by all points whose vector lines end at the same attractor are called basins. In the dynamical systems jargon they are stable manifolds. **QTAIM** selects attractor basins to divide the real space domain. The surface that delimits the basins obeys the zero-flux condition

$$\nabla\rho(\mathbf{r}) \cdot \mathbf{n}(\mathbf{r}) = 0 \qquad \forall \mathbf{r} \in S(\mathbf{r}). \tag{13}$$

QTAIM basins (Ω) define open quantum systems within which the virial theorem is valid.

Topological partitions are distinguished from alternative partitionings for being exhaustive and in real space. Basins recover the whole space, $\mathbb{R}^3 = \cup_A \Omega_A$, while being mutually exclusive, $\Omega_A \cap \Omega_B = \emptyset$.

Properties yield by integration of any monoelectronic quantum operator over **QTAIM** basins are unambiguously assigned to atomic entities. The volume, Ω, and electronic charge, N, of each molecular subunit A are

$$\Omega_{A,\rho} = \int_{\Omega_A} d\mathbf{r}, \qquad N_{A,\rho} = \int_{\Omega_A} \rho(\mathbf{r})\, d\mathbf{r}$$

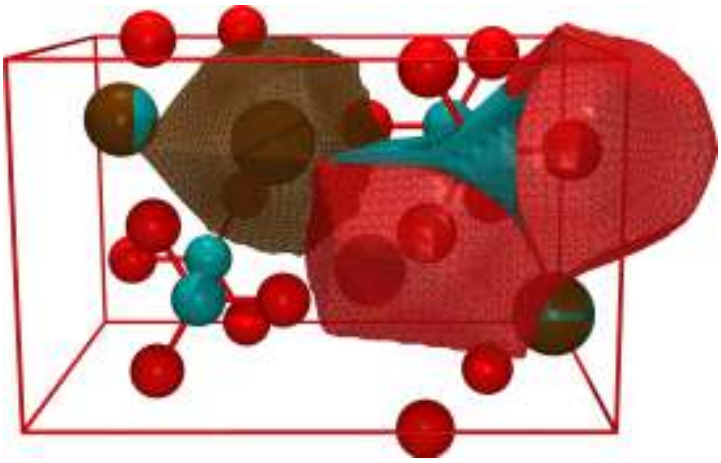

Figure 3: Aragonite structure and its non equivalent atomic basins: Ca (green), C (brown), O (red).

A may be a single atom or an atomic group. The net charge of A is the sum of nuclear and electronic charge, $Q_{A,\rho} = Z_A + N_A$ These formulas will be useful to figure out intermolecular charge transfer in Chapter 4. Moreover, the integration could be over basins of other fields.

2.4 THE ELECTRON DENSITY LAPLACIAN

The Laplacian is a measure of the density field curvature. When the density has a maximum the curvature is negative, $\nabla^2\rho(\mathbf{r}) < 0$, and when it is a minimum the curvature is positive, $\nabla^2\rho(\mathbf{r}) > 0$. Thus, the Laplacian identifies local charge depletions or concentrations.

The values of the Laplacian for an atom oscillate along radial directions, between positive and negative values. The function reveals the atomic shell structure. Each shell has a local maxima and minima along a radial direction. The outer shell is the most important because it is involved in bonding interactions. If it is a charge accumulation shell we call it a Valence Shell Charge Concentration (VSCC), else if it is a charge depletion we call it Valence Shell Charge Depletion (VSCD). Local maximum points $(3,-3)$ and local minima points $(3,+1)$ in VSCC regions are physically interpreted as nucleophilic and electrophilic sites in the acid-base Lewis theory. Critical points are also applied to identify the lone pairs of Valence Shell Electron Pairs Repulsion (VSEPR) theory.

The main characteristic of a covalent bond is that the valence shell electrons are shared. The value of the Laplacian at the bond critical point is negative. Non covalent interactions (e.g. chalcogen, halogen, hydrogen, ionic) involve two closed shell atoms. The Laplacian is

positive at bond critical points and is related to the strength of the interaction.

The results obtained from integration over topological basins are negative [20, 27].

In the next chapter we will focus on the Electrostatic potential.

3 ELECTROSTATIC POTENTIAL

CONTENTS

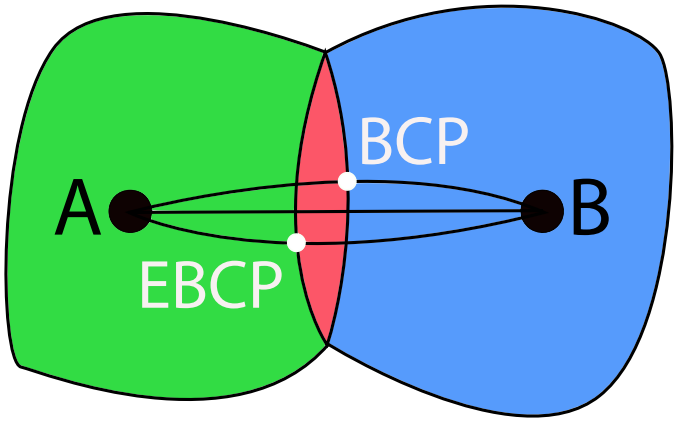

Topology of the electron density and electrostatic potential superimposed. Regions with partial negative (red), neutral (green), and positive (blue) charge conform the basins.

3.1 MEANING OF THE ELECTROSTATIC POTENTIAL

The Molecular Electrostatic Potential (MEP) at a point ($\mathbf{r}$) in space ($\mathbb{R}^3$) is defined as the energy required to bring a positive particle of unit charge from the infinite to that point. In a molecule the potential at infinite is zero by definition, $\phi_0 = \lim_{\mathbf{r}\to\infty}\phi := 0$. It is also the interaction energy between the net charge density of a molecule, $\rho_t(\mathbf{r})$, and a test positive unit particle that mimics a proton, their interaction energy being evaluated without polarization or nuclear rearrangement effects,

$$\phi(\mathbf{r}) := \int_V \frac{\rho_t(\mathbf{r}')}{|\mathbf{r}-\mathbf{r}'|}\,d\mathbf{r}' + \phi_0. \tag{14}$$

The net charge contains the contributions of the electron density distribution and the nuclei $\rho_t(\mathbf{r}) = \sum_A Z_A\delta(\mathbf{r}-\mathbf{R}_A) - \rho(\mathbf{r})$. It is important to note that the Electrostatic Potential is a physical observable that can be determined by X–Ray Diffraction

The seminal paper [6] by Bonaccorsi, Scrocco and Tomasi in 1970 brought attention to the Molecular Electrostatic Potential (MEP) in quantum chemistry for the first time. Since then, many works have emphasized the role of MEP determining the interactions of a molecule with its environment [24]. The interaction between two molecules placed at long distances one apart another is dominated by the electrostatic potential with leading $1/\mathbf{r}$ terms.

The study of the topology of the MEP was started by Gadre *et al.* [29]. Tsirelson identified zero-flux surfaces in solids [39] and Mata and co-workers investigated the zero-flux surfaces and the alternative nucleophilic/electrophilic partitioning [21] using the multipolar model.

Our approach to obtain the Electrostatic Potential (ESP) in a crystal is the same. The electrostatic potential is related to the electronic density by the Poisson equation

$$\nabla^2\phi(\mathbf{r}) = -4\pi\rho_t(\mathbf{r}). \tag{15}$$

Solving for ϕ we obtain equation 14, where nuclei positions are given by structural determination and the electron density by the multipolar model. We cannot recover the potential of reference (ϕ_0), so it is arbitrary. The absolute values of the ESP are arbitrary too, otherwise, the relative values are kept intact.

3.2 PROPERTIES OF THE SCALAR FIELD

The ESP field exhibits the same type of critical points found in the electron density: maxima, minima and saddle points are the most frequent. Thus, the ESP can be characterized by critical points of the gradient field, which is minus the electric field, $\mathbf{E} = -\boldsymbol{\nabla}\phi(\mathbf{r})$.

The zero potential has no effect in the topology.

Cation: A^+—B^+ Neutral: A^-—B^+ Anion: A^-—B

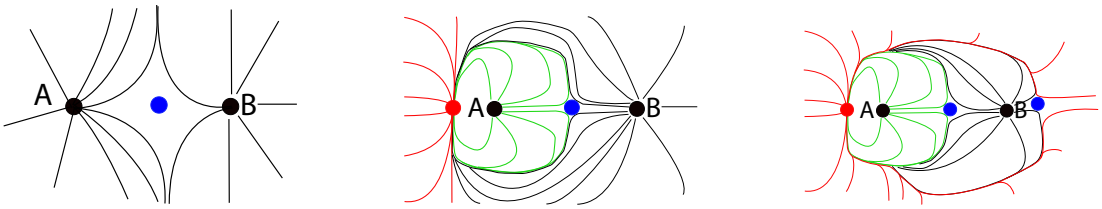

$2-1+0-0=1-0$ $2-1+0-1=1-1$ $2-2+0-1=0-1$

Figure 4: Diagrams of projected electric field lines for hypothetic AB diatomics and the Poincaré-Hopf relationship (17). Zero-flux surfaces have no gradient line crossing them. Critical points appear where gradient lines diverge or converge. Out of the plane critical points also appear, making the interpretation more difficult.

The type is determined by the curvatures of the field γ_i. The

$$\operatorname{diag}(\mathbb{H}_\phi) = \begin{pmatrix} \gamma_1 & 0 & 0 \\ 0 & \gamma_2 & 0 \\ 0 & 0 & \gamma_3 \end{pmatrix}, \tag{16}$$

ESP maxima $(3,-3)$ can only occur at nuclear positions. Minima $(3,+3)$ identify local concentrations of electron density, such as lone pairs. Maxima and minima are identified as nucleophilic and electrophilic sites. $(3,-1)$ saddle points are analogous [10] to density bond critical points.

Maxima are found by the behavior close to the nuclei

In contrast with the electron density, the ESP has positive (electrophilic regions) and negative values (nucleophlic regions). For example, in a cation (see figure 4), gradient field lines go from a positive value at nuclei to zero at infinite. In an anion, gradient field lines go from zero at infinite to a negative value at a localization of electron charge density. In a neutral molecule, gradient lines go from a positive value at nuclei to to infinite and return to end at a minima describing a loop that fills all the space. Therefore, the asymptotic behavior is different and so is the Poincaré–Hopf relationship:

$$n_{-3} - n_{-1} + n_{+1} - n_{+3} = n_+ - n_-. \tag{17}$$

The terms in the left hand side are the number of critical points with signature s (n_s). The terms in the right hand side are the number of asymptotic maxima (n_+) and minima (n_-).

EBCP: *$(3,-1)$ electrostatic bond critical point.*

The Laplacian at a EBCP (figure 5) is related to the total density at that point by the Poisson equation, (18). We can relate the strength of an electrostatic interaction with the value of the Laplacian.

$$\nabla^2\phi = \sum_i^3 \gamma_i = -4\pi\rho_t(\mathbf{r}) = -\nabla\mathbf{E} \tag{18}$$

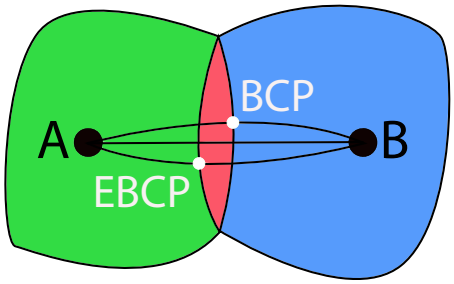

Figure 5: Topology of the electron density and electrostatic potential superimposed. Regions with partial negative (red), neutral (green), and positive (blue) charge conform the basins. Electron density basins of A (green+red) and B (blue) contain their respective atomic charges. ESP basins of A (green) and B (red + blue) are neutral. EBCP appears in the ESP surface. BCP appears in the density basins surface.

Electrostatic, Conservative force, cylindrical symmetry

We can even decompose the electrostatic force in two components, an attractor term along the bond path and a repulsion term perpendicular to the bond using the curvatures of the field.

$$\mathbf{F}_E(\mathbf{r}) = -\rho(\mathbf{r})\mathbf{E} \approx \rho(\mathbf{r})\left[\gamma_{\parallel}(z-z_0)\hat{\mathbf{z}} + \gamma_{\perp} r\hat{\mathbf{r}}\right]$$

Surfaces without any gradient line crossing them define the ESP basins (Λ) [39].

$$\nabla\phi(\mathbf{r})\cdot\mathbf{n}(\mathbf{r}) = -\mathbf{E}(\mathbf{r})\cdot\mathbf{n}(\mathbf{r}) = 0 \qquad \forall \mathbf{r} \in S(\mathbf{r}). \tag{19}$$

Closed basins have no net charge inside [21]. There is no electric field line crossing them. Besides the net charge inside is 0 applying the Gauss theorem.

$$Q_{A,\phi} = \int_{\Lambda_A} \rho_t(\mathbf{r})\, d\mathbf{r} = \int_{S_\phi} \mathbf{E}\cdot\mathbf{n}\, dS := 0. \tag{20}$$

ESP basins have no monopole interactions with the rest of the molecule. An unsolved question is if this property is more general. Does the multipolar expansion converge to zero?

In anions the electron density basins (Λ) enclose ESP basins (Ω). The excess of charge falls outside ESP basins and inside electron density basins, figure 6. The opposite happens for cations. If we compare electron density and ESP basins we can find out where are partial charges located. What is still unknown is if those partial charges can be related to lone pairs or bonds.

The search of zero-flux surfaces and integration over ρ-basins has reached a high level of maturity [17, 34, 38, 40]. Although the ESP field is very similar to the electron density field, some algorithms

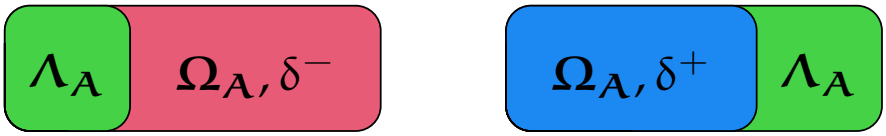

Figure 6: Basins of the electrostatic potential and the electron density. Anion (left), cation (right).

have been specially designed to be used with the electron density and their funcionality has not been tested with other fields. In response, we carried out a preliminary analysis of the electrostatic potential of nitromethane with the `Orca` *ab initio* package. Extracted CUBE grids were analyzed with `critic2`. Our results revealed that the Yu-Trinkle algorithm [40] fails finding the right basins whereas the Henkelman algorithm [34, 38] returns the right partitioning. We used the zero net charge as a quality variable. Another work [1] found also satisfying the results of the Henkelman algorithm for extended systems using *ab initio* and experimental densities as source.

In the case of anions there is a region of space containing the negative charge of the molecule that does not belong to any atom.

At the EBCP the nuclear charge is fully shielded by the electronic distribution. This suggests that the value of the electrostatic potential at the EBCP is related to the strength of the ionic interaction between both atoms. The position of the EBCP can also be related to the electronegativity of the interacting pair of atoms. If $(3,-1)$ points are present in both fields, the relative distance from an atom to the saddle point $d_{A-BCP} > d_{A-EBCP}$ implies that A is more electronegative than B, $\chi_A > \chi_B$.

The potential at the EBCP *is the Coulombic energy generated by the excess of charge (red region in figure 5) of* A *on the other atom (*B *in figure 5)*

3.3 σ-HOLES

The electrostatic potential is positive almost everywhere. Negative regions can be clearly identified as nucleophilic regions that are expected to interact with an electrophile. Electrophilic regions are more difficult to find out because there is no well localized region with positive values. The solution goes through mapping the electrostatic potential on a representative low density isosurface such as the van der Waals surface.

If we map the ESP on a low density isosurface and search for maxima on it we find areas that act as lewis acids and can interact with charge donors . It has been found that in atoms of groups 14 to 17 areas of low density appear on the opposite side of established sigma bonds (see figure 7), called σ-holes, that let the atoms act as acids.

A σ-hole is a low electron density, and therefore relatively positively charged, area adjacent to a σ-bonded element from groups 14 to 17. These areas appear on the opposite side of such atoms to the

bond, along the same axis. The positive charges let the atoms act as Lewis acids, and bond non-covalently with electron donors. In this way σ-holes are located where charge densities provide viable bonding sites between atoms.

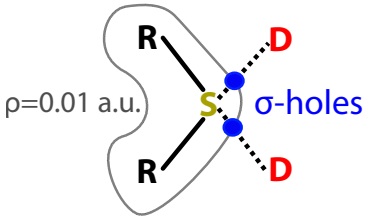

Figure 7: Sigma holes are maxima of the ESP on a low density isosurface.

Part II

Results

4 BTDMTTF–TCNQ MOLECULAR CRYSTAL

CONTENTS

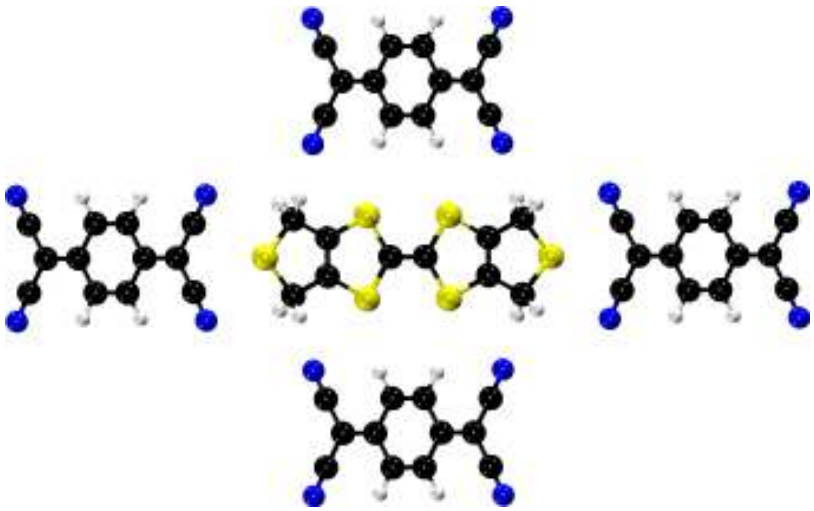

Our crystal is a modification of the historically first organic crystal conductor found.

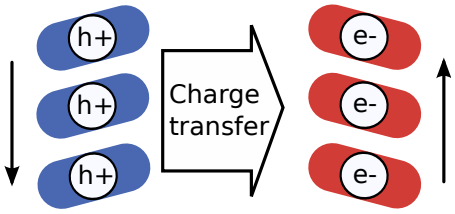

Figure 8: Electrons and holes moving along TCNQ and BTDMTTF columns.

4.1 ORGANIC CONDUCTORS

> It has not yet been achieved, but theoretical studies suggest that it is possible to synthesize **organic materials** that, like certain metals at low temperatures, conduct electricity without resistance.
>
> W. A. Little, 1965

Pure metals and alloys are good conductors but they are expensive and difficult to process. What about organic conductors? The first conductor was found in 1973, co-crystallizing a complex of two different molecules. One is a charge donor and the other is a charge acceptor. Surprisingly, at low temperatures it becomes an insulator instead of a superconductor. The reason is that conduction happens in 1D. Donor and acceptor molecules are stacked as part of columns. Each column has molecules of only one type. Holes move along columns of donor molecules and electrons along acceptor columns (see figure 8). The same transition happens for the system that I will show you, but at a lower temperature.

1973 TTF–TCNQ. First organic metal. Peierls transition at 60 K.

1980 $(TMTSF)_2PF_6$. First organic superconductor.

1993 BTDMTTF–TCNQ. An almost pure 1D metal down to 26 K.

Advantages:

- easy manufacturing
- low cost
- environmental friendly
- mechanical flexibility

4.2 CRYSTAL STRUCTURE DESCRIPTION

The molecular crystal under investigation is a slight modification of the well-known TCNQ-TTF charge-transfer complex, with an addi-

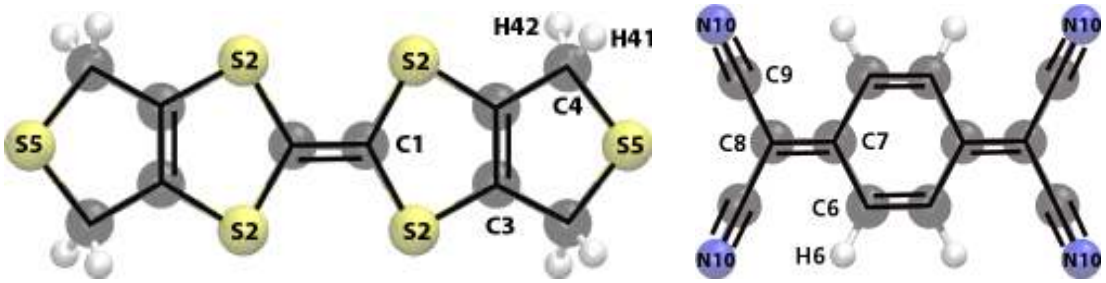

Figure 9: BTDMTTF and TCNQ chemical schemes. The charge transfer magnitude is unknown. It has been previously approximated from multipolar parameters.

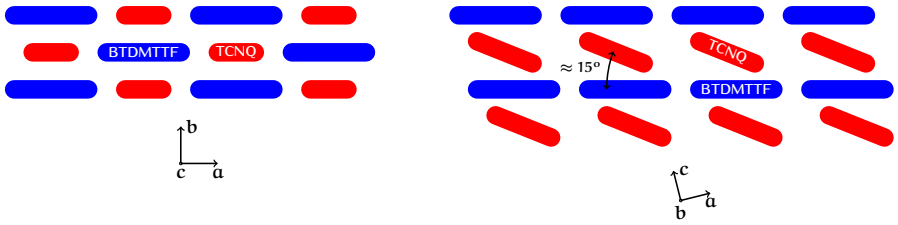

Figure 10: Schematic structure of BTDMTTF–TCNQ.

tional external cycle in the cation. As well as in the former it also presents charge transfer.

The crystal phase structure of BTDMTTF–TCNQ belongs to a monoclinic space group type: $C_{2/m}$. Each column of the 1:1 complex is surrounded by other four of opposite ions (figure 10). They are not stacked at the same c elevation, they are displaced one with respect to another and there is a small angle ($\approx 15^{o}$) between them.

BTDMTTF–TCNQ has a charge transfer excitation from a neutral state to an ionic state with a formal charge transfer of one electron from BTDMTTF to TCNQ (see figure 9). We are interested in calculating it from experimental data at 130 K.

bis(thio-dimethylene)–tetra-thiafulvalene (BTDMTTF)

7,7,8,8–tetracyano-quinodimethane (TCNQ)

The density is obtained from the multipolar parameters fitted against the X-ray structure factors. Hydrogen positions are corrected according to neutron diffraction data. Multipolar parameters refined with `MoPro` are compiled in Appendix A.

A previous work on the system obtained net atomic charges from kappa and multipolar model parameters. The results thereof [8] reported an estimate of the charge transferred upon excitation (q_{CT}) around 0.7 e. Integration over topological basins provides atomic charges with a quantum mechanics grounding.

There is no evidence in the literature to determine what interactions are present, how are they involved in the charge transfer process or how they stabilize the whole crystal structure. Again, a topological analysis can give light on this matter.

`MoProViewer` allows us to analyze critical points and integrate electron density basins. With `critic2` we obtain and integrate electrostatic potential basins.

Our approach consists in selecting a moiety, contributions from other atoms to the density are neglected. We are analyzing atoms isolated but the multipolar parameters are those of the crystal. Appendix B explains the steps followed for the construction of the pseudo-isolated molecules.

However, some density and electrostatic potential basins of isolated molecules are open. The choice of a cluster of an ion embedded inside its nearest neighbors solves the problem.

Previous results remarked that most of the charge transfered is concentrated in nitrogen atoms. And the external sulfur (S5) to C≡N triple bond interactions as the main charge transference pathways.

We will take advantage of electron density, electron density Laplacian, and electrostatic potential topology.

I will analyze several pseudo-isolated molecules: a) each molecule pseudo-isolated b) several dimers to find out what interactions stabilize the structure c) and finally a cluster of each molecule embedded inside its nearest neighbors to achieve closed basins.

4.3 INTRAMOLECULAR INTERACTIONS

When electrons are promoted from donor molecules to acceptor molecules, the cations are stabilized by two resonant structures, one of them is proposed to be more stable due to $4n + 2\pi$ electrons located in its cycle. That structure has internal sulfurs (S2) with sp^2 hybridization. Does it happen the same in this structure? The ratio of electron density field curvatures at BCPs, ellipticity, is used as an indicator of the π character of those interactions.

Property values at (3,-1) critical points of BTDMTTF are collected in table 1. The low values of the density at the BCPs (S2–C1, S2–C3, S5–C4) emphasize the identity of sulfurs as elements isolated from the rest of the molecule. External sulfurs are more isolated than internal sulfurs. The Laplacian is negative indicating that it is a covalent interaction, but the small values indicate that they are close to a non covalent interaction. The electrostatic interaction component is also smaller than other interactions present in the molecule.

The only one interaction with a significant π character is C3-C3'. We see that the original double bond C1-C1 of the neutral BTDMTTF has disappeared.

Nor the internal neither the external sulfur present any π bonding character. It suggests that both have sp^3 hybridization.

The analogy of BCPs and EBCPs is broken by an interaction between internal sulfurs of relative long range.

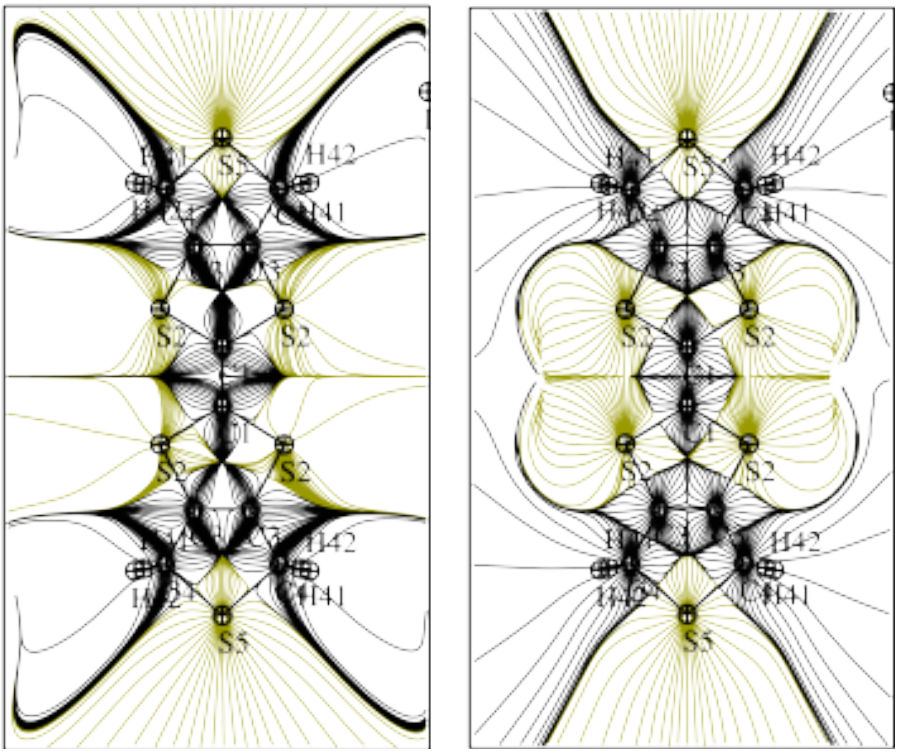

Figure 11: BTDMTTF: Electronic Density (ED) gradient lines (left) follow to the infinite indicating that the molecule is positively charged while some basins of the ESP (right) have a finite surface limit enclosing zero net charge. S5 atoms are not in the plane.

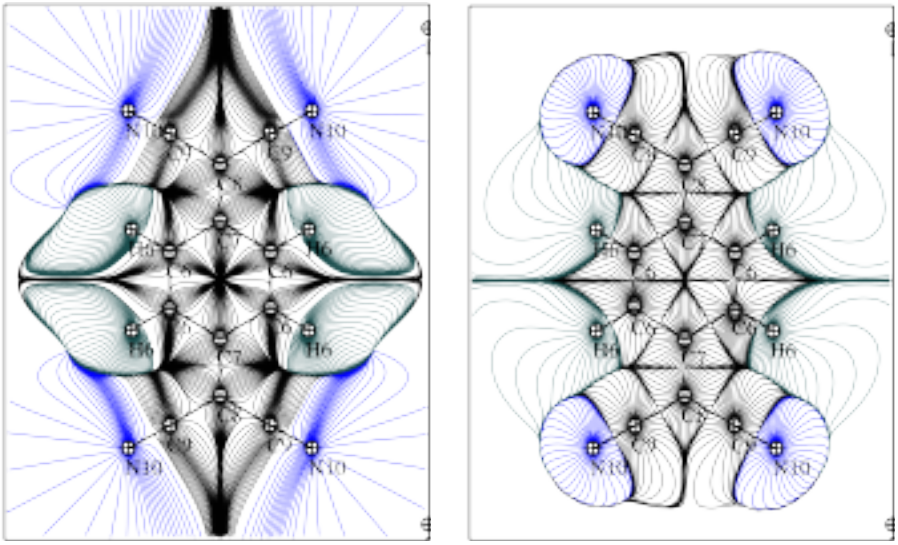

Figure 12: TCNQ: Density (left) and ESP (right) gradient lines. All the atoms are in the plane. Electrostatic Potential field lines are enclosed delimiting a zero charge region.

Table 1: BTDMTTF and TCNQ: Properties of the ED (top block), ρ, and ESP (bottom block), ϕ, scalar fields at $(3,-1)$ critical points between nuclei A and B. d_A and d_B are the distances from the critical point to the positions A and B taken as the length of the straight lines connecting A or B to the CP. Thus $d_{AB} = d_A + d_B$. $\lambda_i(e/Å^5)$ and $\gamma_i(e/Å^3)$ are the curvatures of the density and the electrostatic potential, respectively. As already mentioned in chapter 2 the ordering of curvatures is $\lambda_1 \leqslant \lambda_2 \leqslant \lambda_3$; $\gamma_1 \leqslant \gamma_2 \leqslant \gamma_3$.

ρ: A—B	d_A(Å)	d_B(Å)	d_{AB}(Å)	$\rho(e/Å^3)$	$\nabla^2\rho$	λ_1	λ_2	λ_3	ε
S2—C1	0.968	0.845	1.813	1.275	−0.813	−6.484	−5.483	11.154	0.183
S2—C3	0.849	0.888	1.733	1.341	−2.705	−7.200	−6.240	10.735	0.154
C3—C4	0.728	0.746	1.473	1.765	−10.622	−11.779	−10.427	11.584	0.130
S5—C4	0.960	0.834	1.793	1.131	−0.320	−5.601	−5.205	10.486	0.076
C4—H41	0.794	0.228	1.022	1.667	−18.366	−18.458	−15.763	15.855	0.171
C4—H42	0.795	0.224	1.019	1.675	−16.427	−17.158	−15.669	16.400	0.095
C1—C1′	0.688	0.688	1.376	1.985	−11.046	−12.396	−10.27	11.62	0.207
C3—C3′	0.674	0.674	1.348	2.457	−21.660	−19.705	−13.424	11.469	0.468
N10—C9	0.735	0.424	1.159	3.682	−19.684	−30.801	−27.887	39.004	0.104
C8—C9	0.669	0.748	1.418	1.871	−9.597	−13.042	−10.725	14.170	0.216
C7—C8	0.682	0.718	1.400	1.814	−8.165	−11.442	−10.069	13.346	0.136
C7—C6	0.686	0.750	1.436	1.919	−11.944	−14.027	−10.976	13.059	0.278
C6—H6	1.076	0.037	1.100	1.783	−18.246	−18.757	−14.841	15.352	0.264
ϕ: A—B	d_A(Å)	d_B(Å)	d_{AB}(Å)	$\phi(e/Å)$	$\nabla^2\phi$	γ_1	γ_2	γ_3	
S2—C1	1.030	0.784	1.814	1.163	17.665	−5.192	−5.077	27.934	
S2—C3	0.841	0.797	1.733	1.229	17.498	−6.803	−4.233	28.534	
C3—C4	0.693	0.781	1.473	1.334	23.101	−7.888	−7.104	38.093	
S5—C4	1.000	0.770	1.770	1.044	13.713	−5.216	−3.684	22.613	
C4—H41	0.710	0.443	1.153	1.833	13.452	−19.462	−18.947	51.861	
C4—H42	0.691	0.329	1.019	1.849	16.262	−19.357	−16.635	52.254	
C1—C1′	0.688	0.688	1.375	1.740	27.680	−12.136	−12.009	51.825	
C3—C3′	0.674	0.674	1.348	1.725	33.685	−11.259	−10.632	55.576	
S2—S2′	1.661	1.671	3.330	0.196	1.563	−0.185	−0.073	1.821	
N10—C9	0.582	0.577	1.159	2.404	49.763	−27.129	−20.796	97.688	
C8—C9	0.712	0.706	1.418	1.498	23.766	−10.644	−9.795	44.205	
C7—C8	0.702	0.698	1.400	1.632	25.151	−11.865	−11.017	48.033	
C7—C6	0.720	0.717	1.436	1.382	25.967	−8.758	−8.243	42.968	
C6—H6	0.680	0.397	1.100	1.625	23.063	−19.176	−16.082	58.321	

ESP (3,+3) critical points located in front of nitrogens denote lone pairs location. In the presence of neighbor molecules they disappear.

4.4 INTERMOLECULAR INTERACTIONS

What chemical interactions are present and which one are playing the mayor role? Which is their nature and how one may hope to modify them to improve material's performance? Are these interactions localized or not?

There are two types of intermolecular interactions between columns: frontal and lateral. Frontal interactions involve the external sulfurs (S5) and lateral interactions involve the internal sulfurs (S2), figure 13. The LONGITUDINAL pseudo-isolated dimer is a BTDMTTF cation and its nearest frontal TCNQ anion. The LATITUDINAL pseudo-isolated dimer is a BTDMTTF cation and its nearest lateral TCNQ anion. External sulfurs are displaced out of the cation plane and they are nearly coplanar with the anion. Such displacement is originated by its interactions with TCNQ. It is reasonable to guess that frontal interactions are stronger based upon this observation. Otherwise, we need a more rigorous criteria to assert if any interaction is predominant.

External sulfurs interact with the carbonyl triple bond of the nearest anion, figure 14 (a) interactions, and internal sulfurs interact with the nearest nitrogen (c) and with hydrogens of anions that are above and below (d and e). The sigma hole description resembles correctly the sulfur interactions. The statement that sulfurs have sp^3 hybridization is reinforced. If we apply symmetry and rotate the molecule around the Cl-Cl' bond until we permute internal sulfurs the S2-H interaction points now upside. There is a zigzag interaction between cation and anion stacks connecting S2 lone pairs and hydrogens.

Density values of frontal interactions are greater than those of lateral interactions, table 2. The opposite happens for Laplacian values. Frontal interactions are exceptional, nearly degenerated as its nearly vanishing curvature indicates. The overall of lateral interactions stabilize more the structure.

As well as before, an only electrostatic interaction happens between distant atoms. The ESP is conditionally convergent with the term $\frac{1}{r}$ (monopoles) converging more smoothly than the ED, $\approx e^{-r}$.

There is a substantial difference between nitrogen electron density and electrostatic potential basins, figure 17. The integration of charge inside of the ED but outside of the ESP is a partial negative charge. Therefore, most of the anion net charge is concentrated in nitrogens. They are the main charge acceptors. Where does that charge come from?

There is no big difference between sulfur basins. Besides we cannot assume that external sulfurs donate most of the charge. The sulfur

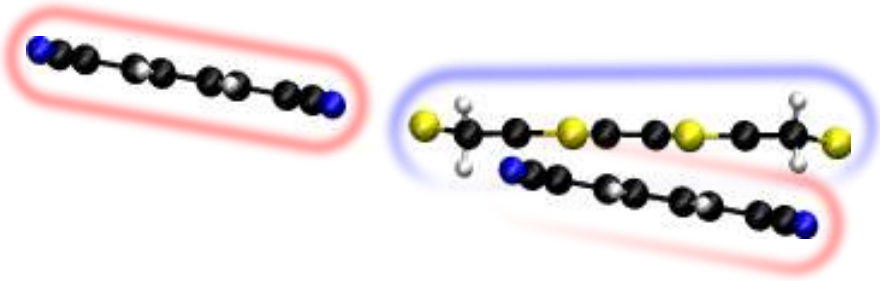

Figure 13: The environment of a BTDMTTF cation: (a) frontal anion and (b) lateral anion constitute the LONGITUDINAL and LATITUDINAL dimers respectively

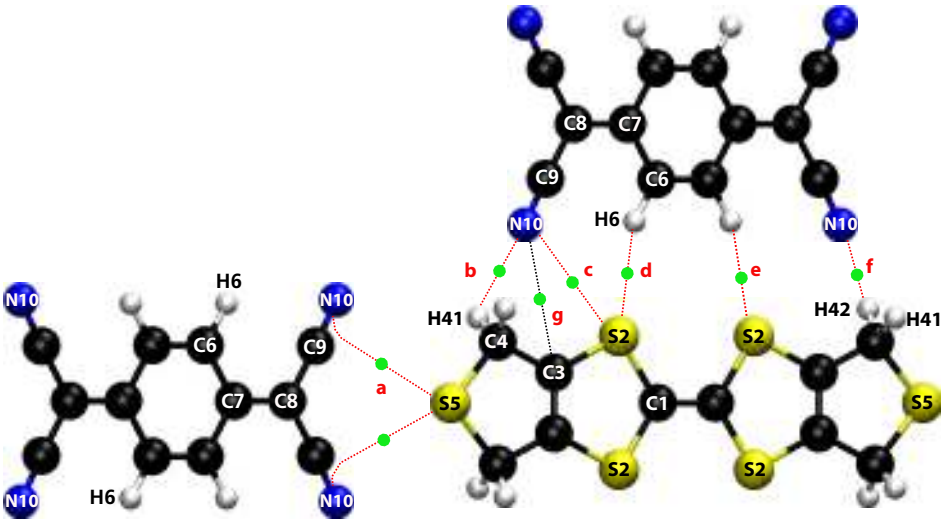

Figure 14: Frontal (a) and lateral (b-g) interactions. There is an only electrostatic interaction (g).

ρ-basin total charge is close to zero. Hydrogens and internal sulfurs might play a more important role in charge transfer than expected.

In addition to interactions involving molecules of different stacks there are also π–π interactions along the chain of molecules in the columns, figure 18,17.

Sulfurs are given to establish many weak connections with other sulfurs (see table 3). Most of them are between equivalent atoms, therefore they are not relevant to charge transfer. They are not traditional VSCD to VSCC.

4.5 CHARGE TRANSFER

All previous pseudo-isolated molecules share a common fact: some basins are open. We have to handle this fact if we are interested in integrating atomic partial and total charges without neglecting the

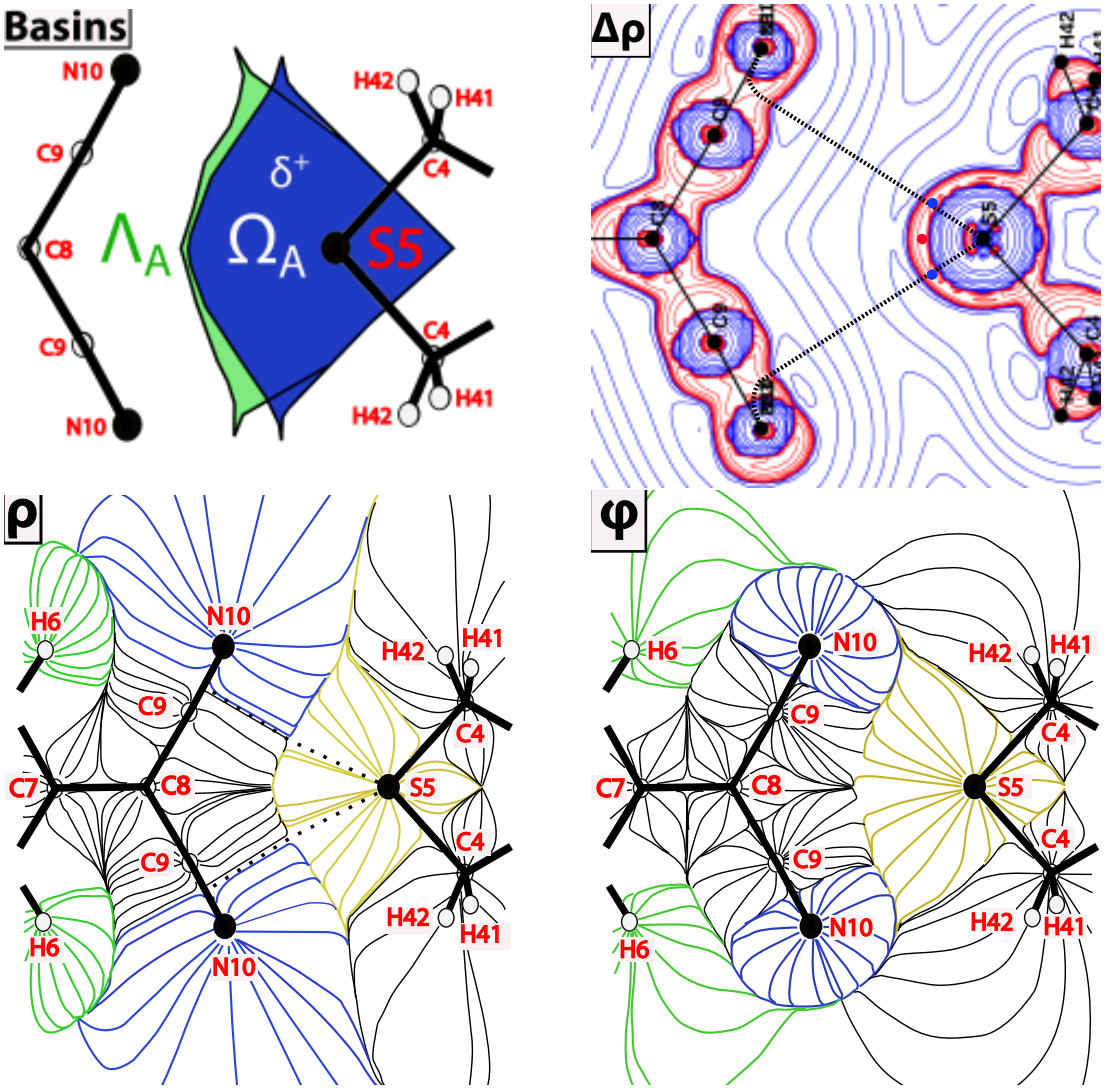

Figure 15: LONGITUDINAL: Density (left) and ESP (middle) gradient lines. The volume of nitrogen density basins is greater than ESP basins. Nitrogens accumulate a negative charge. S5 basin volume is almost not changed. The S5–triple bond path goes between N and C9 basins. Nearly degenerated. Plane of S5 and two N10.

Table 2: Properties of $(3,-1)$ critical points in the LONGITUDINAL and the LATITUDINAL dimer. The meaning of variables is the same as set for table 1. The value of the Laplacian, $\nabla^2\rho(e/Å^5)$ and $\nabla^2\phi(e/Å^3)$, for intermolecular interactions can be included due to a lower density variability with small position modifications.

ρ: A ··· B	d_A(Å)	d_B(Å)	d_{AB}(Å)	$\rho(e/Å^3)$	$\nabla^2\rho$	λ_1	λ_2	λ_3
C9≡N10 ··· S5	1.739	1.761	3.439	0.402	0.534	−0.090	−0.055	0.679
H41 ··· N10	1.056	1.466	2.522	0.062	0.949	−0.206	−0.163	1.318
S2 ··· N10	1.686	1.528	3.214	0.049	0.645	−0.125	−0.113	0.884
S2 ··· H6	2.057	1.285	3.342	0.013	0.232	−0.030	−0.020	0.283
S2′ ··· H6′	1.965	1.350	3.315	0.020	0.262	−0.055	−0.042	0.359
H42 ··· N10	1.022	1.571	2.593	0.030	0.609	−0.105	−0.098	0.812
ϕ: A ··· B	d_A(Å)	d_B(Å)	d_{AB}(Å)	$\phi(e/Å)$	$\nabla^2\phi$	γ_1	γ_2	γ_3
C9≡N10 ··· S5	1.574	1.860	3.390	0.031	0.460 7	−0.191	−0.107	0.758
C3 ··· N10	2.537	0.988	3.525	1.639	3.625	−0.887	−0.755	5.267
S2 ··· H6	2.330	1.021	3.351	1.248	0.231	−0.491	−0.417	1.139

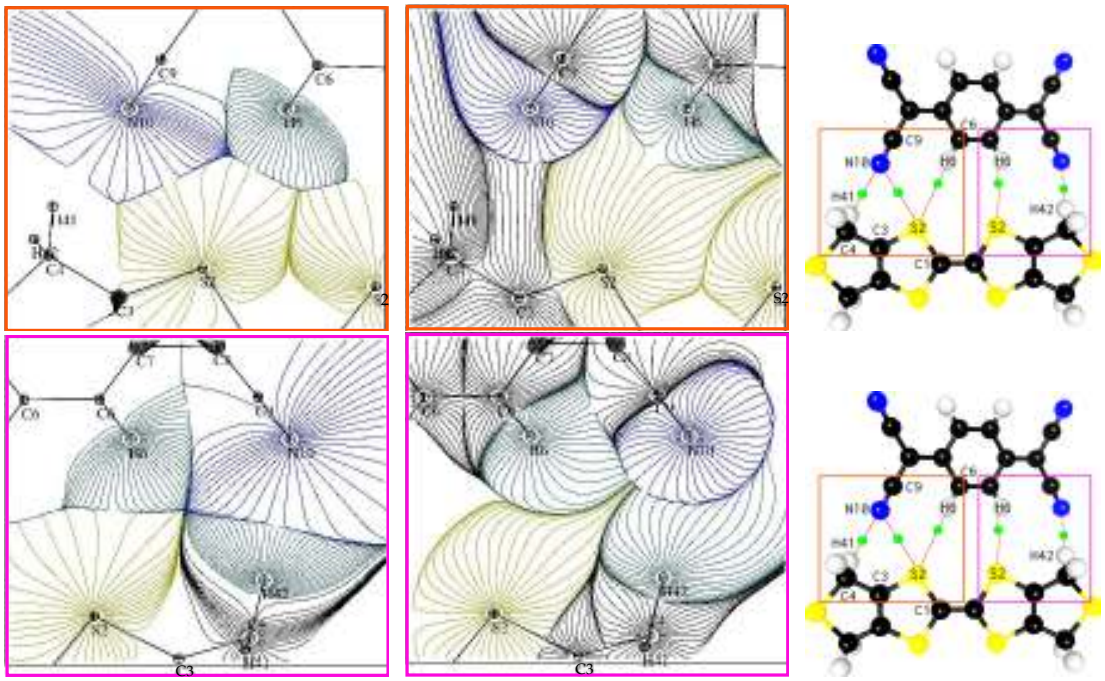

Figure 16: LATITUDINAL: Density and ESP gradient lines. Top images represent the plane N10-H6-S2. Bottom images represent the plane N10-H41-S2.

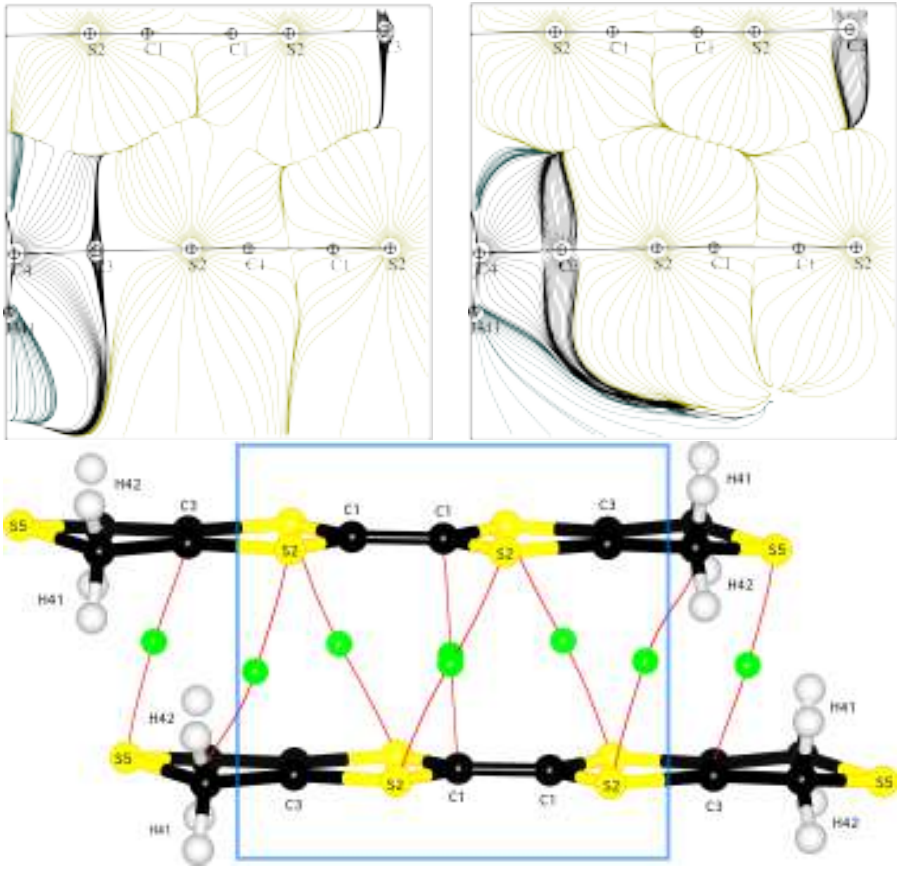

Figure 17: BTDMTTF stack: Density and ESP gradient lines. Planes defined by 4 S2 atoms.

Table 3: BTDMTTF and TCNQ stacks: Density and ESP (3, −1) critical points. The meaning of variables is the same as set for table 1.

ρ: A ··· B	d_A(Å)	d_B(Å)	d_{AB}(Å)	ρ(e/Å^3)	$\nabla^2\rho$	λ_1	λ_2	λ_3
S2 ··· S2′	1.944	1.944	3.888	0.035	0.297	−0.074	−0.019	0.391
S2 ··· S2″	1.948	1.931	3.879	0.035	0.324	−0.056	−0.034	0.414
S2 ··· C4	1.925	1.867	3.792	0.037	0.329	−0.081	−0.025	0.435
C1 ··· C1	1.757	1.757	3.514	0.036	0.352	−0.033	−0.023	0.407
S5 ··· C3-C3	1.803	1.671	3.474	0.045	0.413	−0.091	−0.032	0.536
C7 ··· C7	1.649	1.649	3.298	0.047	0.478	−0.062	−0.016	0.555
C8 ··· C7	1.640	1.639	3.279	0.048	0.501	−0.071	−0.022	0.595
ϕ: A ··· B	d_A(Å)	d_B(Å)	d_{AB}(Å)	ϕ(e/Å)	$\nabla^2\phi$	γ_1	γ_2	γ_3
H41 ··· H42	1.190	1.268	2.458	0.424	0.230	−0.345	−0.302	0.877
S2 ··· H42	1.800	1.466	3.266	0.342	0.186	−0.219	−0.140	0.545
S2 ··· S2′	1.997	1.998	3.995	0.193	0.159	−0.107	−0.046	0.311

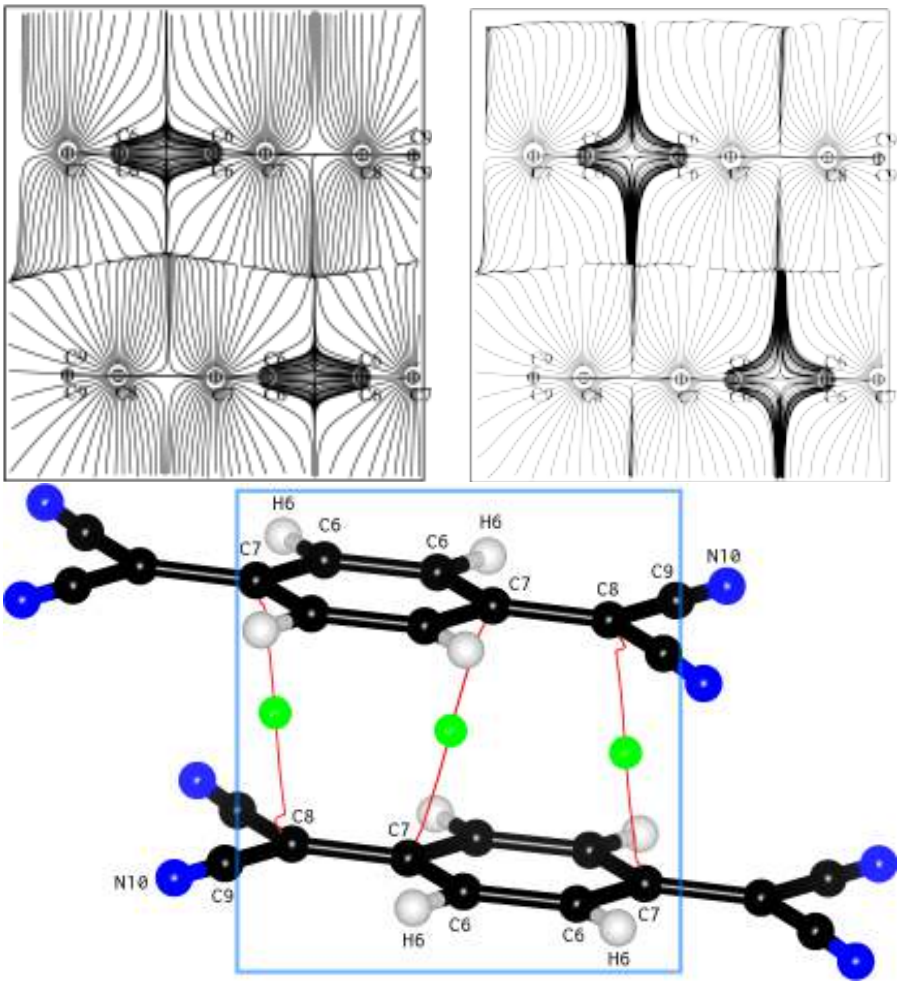

Figure 18: TCNQ stack: Density and ESP gradient lines. Planes defined by C7 and C8 atoms.

integration far from the nuclei. Taking a cluster, the basins of the inner molecule are finite because it is completely surrounded.

Anions and cations are stacked as columns along the c axis. Each anion or cation is surrounded by 8 counterpart ions in the ab crystallographic planes and two equals along the c direction.

The left side of the table 4 are properties of the cation and the right side are properties of the anion. The integrated charges of molecules are in close agreement with multipolar (Q′) and kappa (Q″) populations. The agreement vanishes when we compare atomic charges. For example, C9 and N10 of carbonyl groups. However, refined charges are good for chemical groups (e.g. CN), or molecules.

Nitrogens have a partial charge close to 1 e, but most of the charge is transfered from the contiguous carbon (C9). Sulfurs and hydrogens of BTDMTTF contribute equally to charge donation.

The negative charge of N10 is located inside a large volume whereas the positive charge of internal sulfurs is located in a very small volume. As an average the density is high inside that region of space.

The integration of the density in the ESP basins is good. We loss 2 e in the integration. It is about 0.008 e/basin.

The charge transfer from the integration is 0.63 whereas the values from two multipolar refinements published beforehand are close and sugest us that for chemical groups those parameters estimate right values. If we take a look at both the partial atomic charges and the volume difference between the density and ESP basins we can estimate the localization partial charges. Thus for the S2 atom we can see that the charge is highly concentrated in a small region of space.

S5 basins volume are scarcely different as we expected from plane sections outlined before.

The charge inside ESP basins is 0 (minor numerical errors) as it should be.

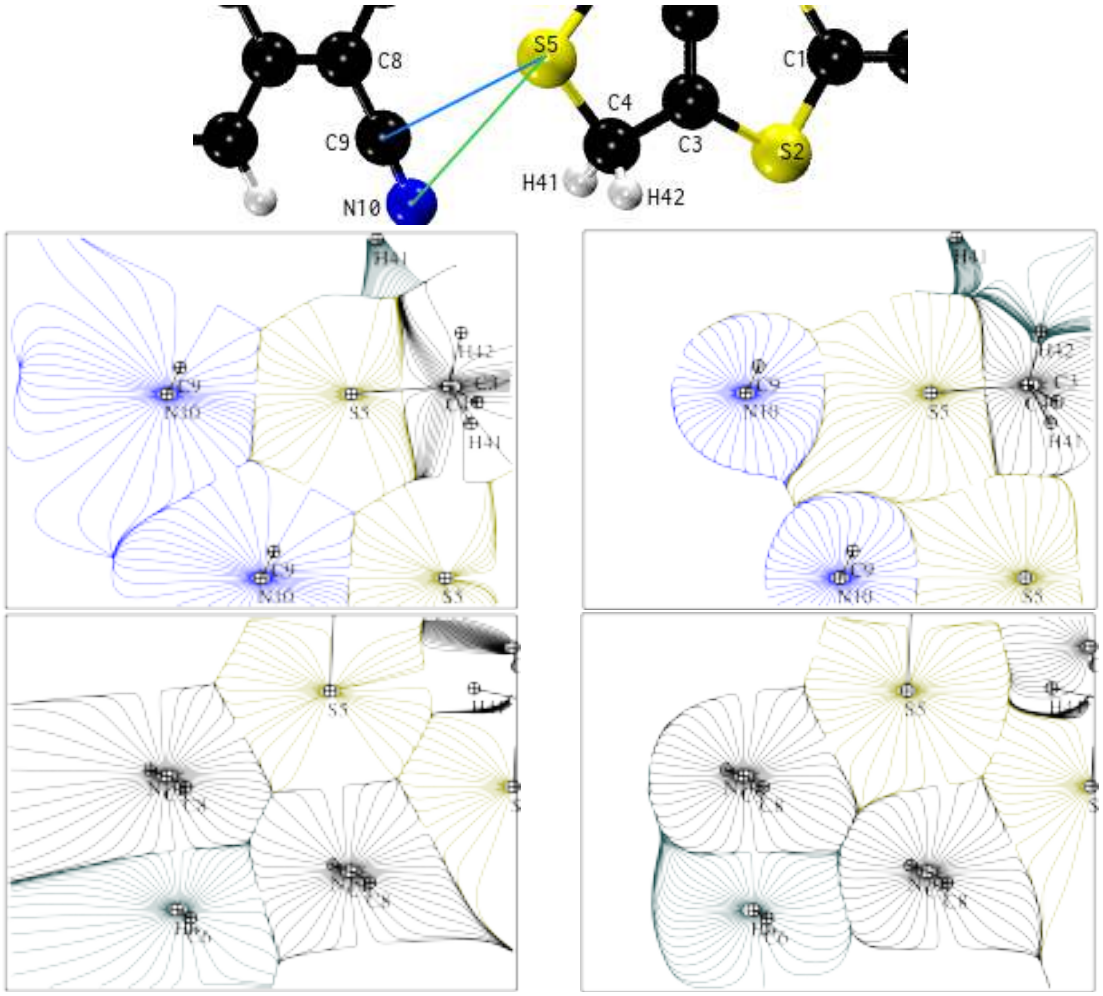

Figure 19: Interactions of S5 with anion atoms. Top planes defined by S5 and two N10 atoms. Bottom planes defined by S5 and two C9 atoms.

There is a huge polarization of the C9–N10 bond. Curiously, there is no Laplacian zero isosurface between them. The charge depletion along the bond path at the BCP is very high but the charge concentration along the other two directions is also big. The charge concentration between the two atoms is hight but inside the N basin.

The charge is polarized but the IAS is very close to the C9. The value of the curvatures is very high.

Integration of the density — I used the valence — inside the electrostatic potential basins is 0 within a maximum error of 0.07 e.

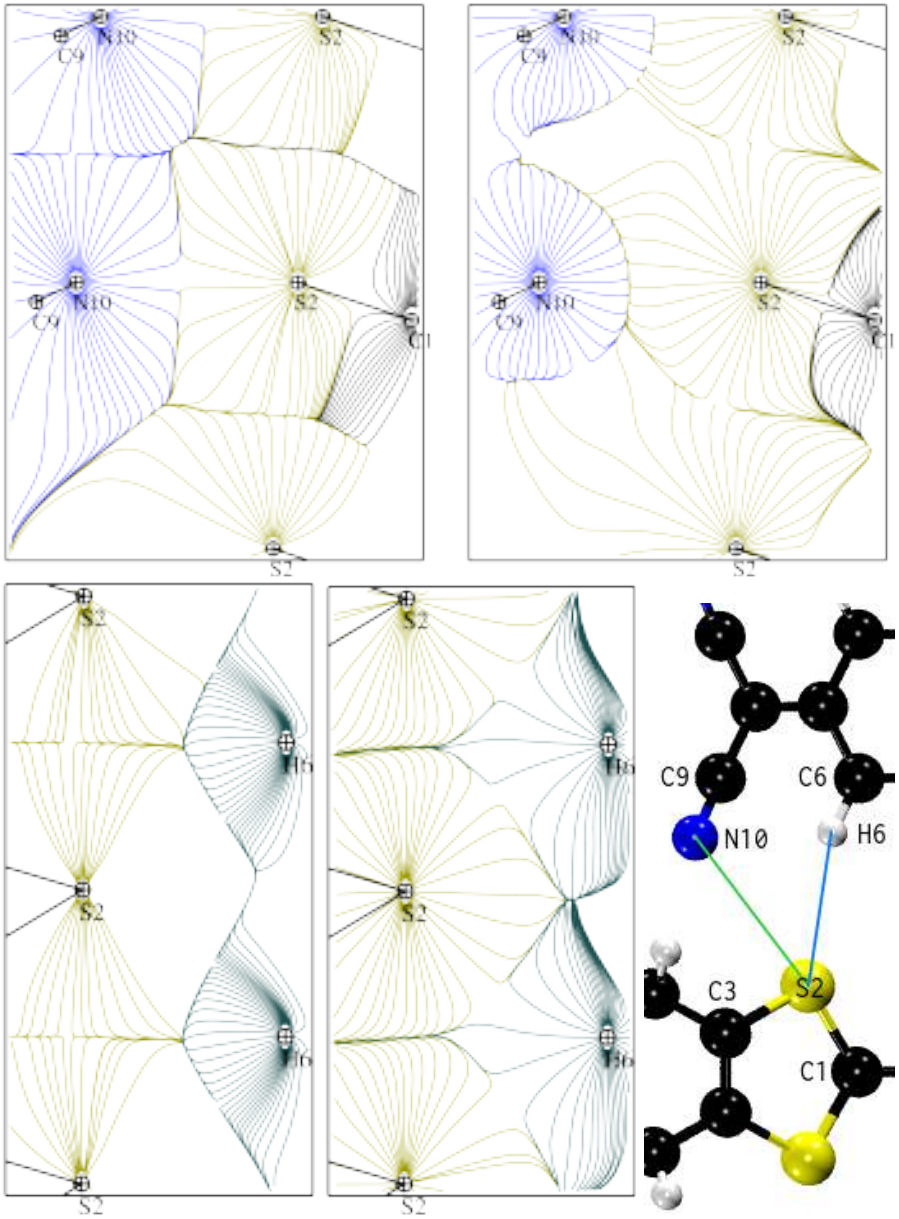

Figure 20: Interactions of S2 with anion atoms. Planes coplanar to S2 and N10 atoms; planes coplanar to S2 and H6 atoms.

Table 4: ED integration inside density basins (Ω) (top block) and ESP basins (Λ) (bottom block) of the inner molecule of the BTDMTTF cluster (left) and TCNQ cluster (right). Q' and Q'' taken from [8]. * Total refers to the whole molecule (BTDMTTF or TCNQ).

A	Ω_A(Å^3)	Q_{Ω_A}(e)	Q'(e)	Q''(e)	A	Ω_A(Å^3)	Q_{Ω_A}(e)	Q'(e)	Q''(e)
S2	23.263	0.375	0.365	0.356	N10	25.285	−0.973	−0.139	−0.135
C3	9.608	−0.245	−0.171	−0.178	C6	11.537	−0.179	−0.045	−0.039
C4	12.841	−0.516	−0.500	−0.512	C7	8.821	0.026	0.088	0.092
H41	5.060	0.288	0.251	0.259	C8	9.598	−0.020	−0.074	−0.066
H42	5.272	0.358	0.300	0.301	C9	4.613	0.767	−0.075	−0.071
S5	21.961	0.241	0.328	0.336	H6	6.105	0.230	0.045	−0.039
C1	10.616	−0.442	−0.444	−0.454					
Total*	289.33	0.63	0.75	0.67	Total*	227.00	−0.62	−0.75	−0.67
A	Λ_A(Å^3)	Q_{Λ_A}(e)			A	Λ_A(Å^3)	Q_{Λ_A}(e)		
S2	23.691	0.002			N10	8.749	0.006		
C3	7.803	0.003			C6	10.551	−0.006		
C4	8.750	−0.004			C7	7.926	0.010		
H41	10.888	0.009			C8	8.412	−0.009		
H42	12.890	−0.005			C9	13.416	−0.005		
S5	25.073	0.005			H6	11.074	0.014		
C1	6.803	0.006							
Total*	319.84	0.042			Total*	207.84	0.038		

Part III

Conclusions

5 CONCLUSIONS

- A more accurate value of intermolecular charge transfer (0.62–0.63 e) is reported.
- While charges inferred from multipoles replicate integrated charges for coarse grained atomic groups, they fail when fine granularity (e.g. C, N) is demanded.
- Contributions to charge transfer are spread amongst several atoms instead of being localized in sulphur atoms, as previously pointed out. Delocalization indices could be approximated with a functional. DFT calculation: GGA functionals fail. We should try with the VASP HSE functional.
- We have systematically identified the interactions present in the crystal phase using also the topology of the electrostatic potential and the laplacian of the electron density with the mopro and critic programs. Some π-π interactions are like halogen type I ones. Their nature is not well understood till today.
- The intersection of density and potential basins allows us to determine the concentration of partial charges.
- Each sulphur has 5 intermolecular interactions. The capacity of sulphurs to stabllish interactions is fullfilled.

Part IV

Appendix

A MULTIPOLAR PARAMETERS

All the results of chapter 4 are based on the Hansen–Coppens model. The parameters of the model are listed in table 5. Atoms labeling is in figure 21.

Symmetry restrictions [18, 19] reduce the number of multipolar moments to be fitted. The choice of local co-ordinate axes must be adequate.

Hydrogen atoms have multipolar parameters until $l = 2$. First row elements until $l = 3$. Second row elements and so on until $l = 4$. Continuing with the multipolar expansion is non sense because they have each time a less clear physical meaning.

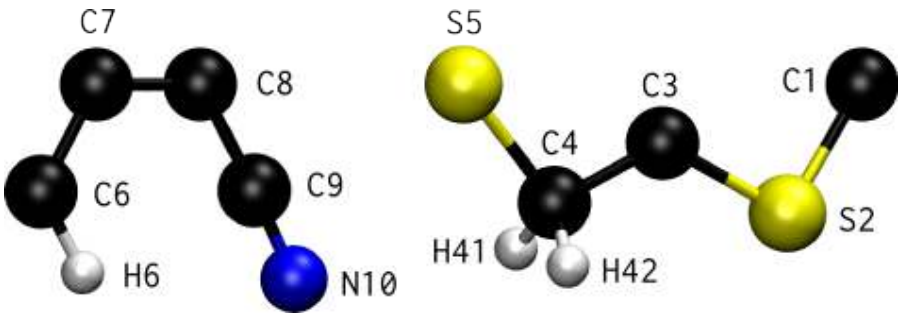

Figure 21: Only a quarter of each molecule is contained in the asymmetric unit.

Table 5: Electronic density multipolar parameters of atoms belonging to the asymmetric unit. All P_{00} monopoles are 0. Atomic charges can be estimated with $q = Z - (N_{core} + P_{val} + P_{00})$.

	S2	S5	N10	C1	C3	C4	C6	C7	C8	C9	H41	H42	H6
κ	1.077 3	1.078 0	1.009 0	0.995 5	1.016 2	0.988 5	1.021 5	1.027 1	1.028 6	1.040 2	1.182 1	1.162 0	1.070 0
κ'	1.054 6	1.101 9	0.999 3	0.983 4	0.971 7	0.966 4	0.982 5	1.006 1	0.974 2	0.968 9	0.895 1	1.009 4	1.049 2
P_{val}	5.644	5.664	5.135	4.454	4.178	4.512	4.039	3.908	4.066	4.071	0.741	0.700	0.935
P_{11}	−0.066	−0.031	−0.022	0.033	0.014	−0.006	−0.003	−0.016	0.046	−0.173	0.107	0.092	0.143
$P_{1\bar{1}}$	−0.058	0.007	0.004	0.005	−0.026	−0.088	0.010	−0.012	0.009	0.0	0.0	0.0	0.0
P_{10}	0.011	0.0	−0.035	0.0	−0.003	0.008	0.017	0.0	0.0	−0.050	0.0	0.0	0.0
P_{20}	−0.025	0.009	−0.118	0.034	−0.212	0.035	−0.250	0.062	0.038	−0.239	0.0	0.0	0.0
P_{21}	0.0	0.0	−0.017	0.0	0.006	0.043	0.004	0.0	0.0	0.015	0.0	0.0	0.0
$P_{2\bar{1}}$	−0.001	0.0	0.029	0.0	−0.008	0.006	0.0	0.0	0.0	−0.016	0.0	0.0	0.0
P_{22}	−0.041	−0.029	0.215	0.109	−0.059	−0.041	0.0	0.085	0.074	0.311	0.0	0.0	0.0
$P_{2\bar{2}}$	0.141	0.019	−0.017	0.012	0.046	0.102	−0.023	0.008	0.0	−0.067	0.0	0.0	0.0
P_{30}	0.002	0.0	0.007	0.0	−0.013	−0.017	−0.004	0.0	0.0	−0.004			
P_{31}	−0.047	0.052	−0.026	0.125	−0.038	−0.192	−0.013	−0.116	−0.131	−0.014			
$P_{3\bar{1}}$	−0.038	−0.014	−0.012	0.017	−0.040	−0.234	0.031	−0.010	0.009	−0.023			
P_{32}	0.002	0.0	0.019	0.0	−0.005	−0.019	0.015	0.0	0.0	0.014			
$P_{3\bar{2}}$	0.006	0.0	0.002	0.0	−0.002	0.009	−0.002	0.0	0.0	0.019			
P_{33}	0.088	0.014	0.041	−0.014	0.263	0.183	0.298	0.011	0.043	0.028			
$P_{3\bar{3}}$	0.062	0.0	0.031	0.017	−0.031	0.050	−0.001	−0.005	−0.009	0.002			
P_{40}	0.083	0.003											
P_{41}	0.049	0.0											
$P_{4\bar{1}}$	−0.026	0.0											
P_{42}	−0.026	0.025											
$P_{4\bar{2}}$	0.011	0.007											
P_{43}	−0.008	0.0											
$P_{4\bar{3}}$	−0.080	0.0											
P_{44}	0.043	0.033											
$P_{4\bar{4}}$	−0.005	−0.036											

B GENERATION OF PSEUDOISOLATED MOLECULES

The symmetry space group is $C_{2/m}$.

The centering vectors are:

$$v_1 = \left\{ \begin{array}{ccc|c} 0 & 0 & 0 & 0 \\ 0 & 0 & 0 & 0 \\ 0 & 0 & 0 & 0 \end{array} \right\} \qquad v_2 = \left\{ \begin{array}{ccc|c} 0 & 0 & 0 & 1/2 \\ 0 & 0 & 0 & 1/2 \\ 0 & 0 & 0 & 0 \end{array} \right\} \tag{21}$$

These instructions are mainly oriented towards the use of moproviewer. The symmetry operations that correspond to the space group are in the table 6. The set of operations:

$$P = \{E, \sigma\}; \qquad Q = \{i, C_2\}; \tag{22}$$

$$P^2 = \{E + v_2, \sigma + v_2\}; \qquad Q^2 = \{i + v_2, C_2 + v_2\}, \tag{23}$$

will shorten the list.

What follows is a collection of all isometry combinations needed to construct those structures from the asymmetric unit.

B.1 BTDMTTF

The molecule is generated with the symmetry operations $P, Q + (2, 0, 0)$ to the asymmetric unit.

B.2 TCNQ

The operations are: $P, Q + (1, 0, 1)$

Table 6: Symmetry operations of the BTDMTTF–TCNQ crystal.

Chemical notation	Steitz operator	Ortep code
E	$\left\{\begin{array}{ccc\|c} 1 & 0 & 0 & 0 \\ 0 & 1 & 0 & 0 \\ 0 & 0 & 1 & 0 \end{array}\right\}$	55501
$\sigma(ac)$	$\left\{\begin{array}{ccc\|c} 1 & 0 & 0 & 0 \\ 0 & -1 & 0 & 0 \\ 0 & 0 & 1 & 0 \end{array}\right\}$	55502
i	$\left\{\begin{array}{ccc\|c} -1 & 0 & 0 & 0 \\ 0 & -1 & 0 & 0 \\ 0 & 0 & -1 & 0 \end{array}\right\}$	55551
$C_2(b)$	$\left\{\begin{array}{ccc\|c} -1 & 0 & 0 & 0 \\ 0 & 1 & 0 & 0 \\ 0 & 0 & -1 & 0 \end{array}\right\}$	55552

B.3 LONGITUDINAL DIMER

Figure 22: LONGITUDINAL dimer: Top image of the dimer represents a c axis perspective. Bottom image is along the b axis.

The structure represented in figure 22 is generated with the operations $P, Q + (1, 0, 1)$, $P + (-1, 0, 2), Q + (1, 0, 2)$.

B.4 LATITUDINAL DIMER

The structure represented in figure 23 is generated with the operations $P, Q + (2, 0, 0)$ $P^2, Q^2 + (1, 0, 0)$

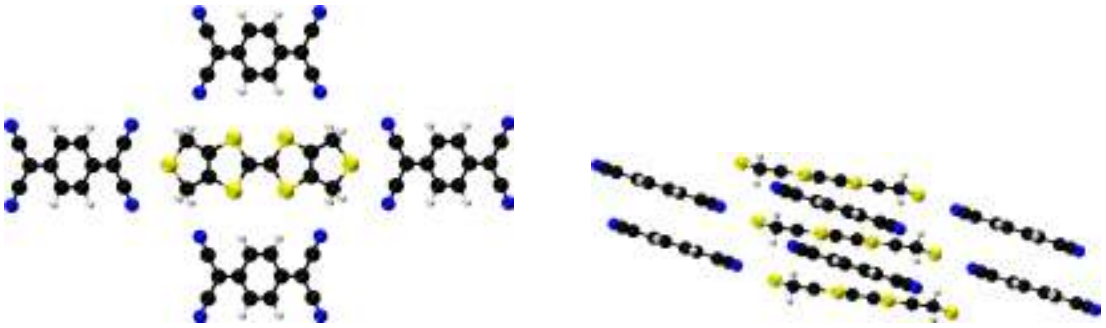

Figure 24: BTDMTTF cluster: Left image is along the c axis and right image is along the b axis.

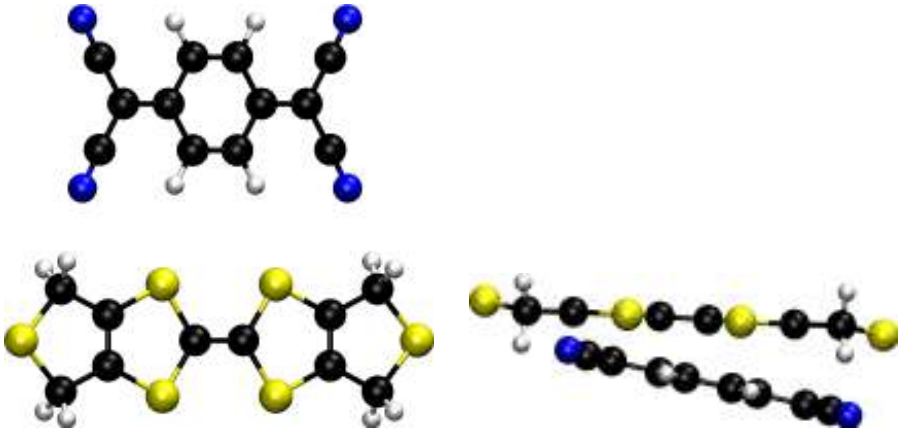

Figure 23: LATITUDINAL dimer: Left image is along the c axis and right image is along the b axis.

B.5 BTDMTTF DIMER STACK

$P, Q + (2, 0, 0)$
$P + (0, 0, 1), Q + (2, 0, 1)$

B.6 TCNQ DIMER STACK

$P, Q + (1, 0, 1)$
$P + (-1, 0, 2), Q + (1, 0, 2)$
$P + (0, 0, -1), Q + (2, 0, -1)$

B.7 BTDMTTF CLUSTER

Structure of figure 24.
Operations:
$P, Q + (1, 0, 1)$

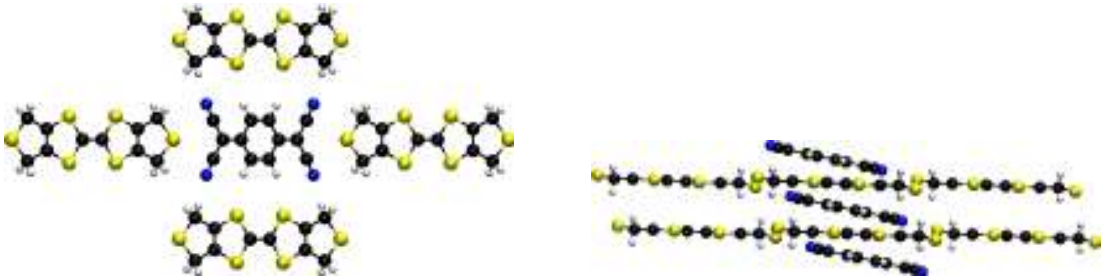

Figure 25: TCNQ cluster: Left image is along the c axis and right image is along the b axis.

$P + (0,0,1), Q + (1,0,2)$
$P + (0,0,-1)$
$Q^2 + (1,0,0), P^2$
$Q^2 + (1,0,1), P^2 + (0,0,-1)$
$Q^2 + (1,-1,0), P^2 + (0,-1,-1)$
$Q^2 + (1,-1,1), P^2 + (0,-1,-1)$
$P + (1,0,0), Q + (2,0,-1)$
$P + (1,0,-1), Q + (2,0,0)$
$P + (1,0,-2), Q + (2,0,1)$

B.8 TCNQ CLUSTER

The structure of figure figure 25.
Operations: $P, Q + (1,0,1)$
$P + (0,0,1), Q + (1,0,2)$
$P + (0,0,-1)$
$Q^2 + (1,0,0), P^2$
$Q^2 + (1,0,1), P^2 + (0,0,-1)$
$Q^2 + (1,-1,0), P^2 + (0,-1,-1)$
$Q^2 + (1,-1,1), P^2 + (0,-1,-1)$ $E, \sigma, i + (1,0,1), C_2 + (1,0,1)$

Part V

Bibliography

BIBLIOGRAPHY

[1] Aubert, E., Lebègue, S., Marsman, M., Bui, T. T. T., Jelsch, C., Dahaoui, S., Espinosa, E. and Ángyán, J. G. (2011), «Periodic Projector Augmented Wave Density Functional Calculations on the Hexachlorobenzene Crystal and Comparison with the Experimental Multipolar Charge Density Model», *The Journal of Physical Chemistry A*, vol. 115 (50), pp. 14 484–14 494, URL http://pubs.acs.org/doi/abs/10.1021/jp206623x. {Cited on page 27.}

[2] B. Silvi, A. S. (1994), «Classification of chemical bonds based on topological analysis of electron localization functions», *Nature*, vol. 371, pp. 683–686, URL http://dx.doi.org/10.1038/371683a0. {Cited on page 17.}

[3] Bader, R. (1994), *Atoms in Molecules: A Quantum Theory*, International Ser. of Monogr. on Chem, Oxford University Press, Incorporated. {Cited on pages xi and 16.}

[4] Bader, R. F. W. (2011), «Worlds Apart in Chemistry: A Personal Tribute to J. C. Slater», *The Journal of Physical Chemistry A*, vol. 115 (45), pp. 12 667–12 676, URL http://pubs.acs.org/doi/abs/10.1021/jp203531x. {Cited on page 16.}

[5] Berlin, T. (1951), «Binding Regions in Diatomic Molecules», *The Journal of Chemical Physics*, vol. 19 (2), pp. 208–213, URL http://scitation.aip.org/content/aip/journal/jcp/19/2/10.1063/1.1748161. {Cited on page 16.}

[6] Bonaccorsi, R., Scrocco, E. and Tomasi, J. (1970), «Molecular SCF Calculations for the Ground State of Some Three-Membered Ring Molecules: (CH2)3, (CH2)2NH, (CH2)2NH2+, (CH2)2O, (CH2)2S, (CH)2CH2, and N2CH2», *The Journal of Chemical Physics*, vol. 52 (10), pp. 5270–5284, URL http://scitation.aip.org/content/aip/journal/jcp/52/10/10.1063/1.1672775. {Cited on page 24.}

[7] Coppens, P. (1997), *X-Ray Charge Densities and Chemical Bonding*, International Union of Crystallography Texts on Crystallography, Oxford University Press, USA. {Cited on pages 11 and 12.}

[8] Espinosa, E., Molins, E. and Lecomte, C. (1997), «Electron density study of the one-dimensional organic metal bis(thiodimethylene)-tetrathiafulvalene tetracyanoquinodimethane», *Phys. Rev. B*, vol. 56, pp. 1820–1833, URL

http://link.aps.org/doi/10.1103/PhysRevB.56.1820. {Cited on pages xi, 33, and 46.}

[9] Francisco, E., Pendás, A. M., García-Revilla, M. and Boto, R. Á. (2013), «A hierarchy of chemical bonding indices in real space from reduced density matrices and cumulants», *Computational and Theoretical Chemistry*, vol. 1003 (0), pp. 71–78, URL http://www.sciencedirect.com/science/article/pii/S2210271X12004756. {Cited on page 17.}

[10] Gadre, S. R. and Bendale, R. D. (1986), «On the similarity between molecular electron densities, electrostatic potentials and bare nuclear potentials», *Chemical Physics Letters*, vol. 130 (6), pp. 515 – 521, URL http://www.sciencedirect.com/science/article/pii/0009261486802494. {Cited on page 25.}

[11] Gatti, C. and Macchi, P., eds. (2012), *Modern Charge-Density Analysis*, Springer. {Cited on pages 1 and 3.}

[12] Hahn, T., ed. (2002), *International tables for crystallography, vol. A*, International Union of Crystallography by Kluwer Academic Publishers. {Cited on page 8.}

[13] Hansen, N. K. and Coppens, P. (1978), «Testing aspherical atom refinements on small-molecule data sets», *Acta Crystallographica Section A*, vol. 34 (6), pp. 909–921, URL http://dx.doi.org/10.1107/S0567739478001886. {Cited on page 11.}

[14] Hernández-Trujillo, J. and Bader, R. F. W. (2000), «Properties of Atoms in Molecules: Atoms Forming Molecules», *The Journal of Physical Chemistry A*, vol. 104 (8), pp. 1779–1794, URL http://pubs.acs.org/doi/abs/10.1021/jp994096z. {Cited on page 17.}

[15] Jelsch, C., Guillot, B., Lagoutte, A. and Lecomte, C. (2005), «Advances in protein and small-molecule charge-density refinement methods using *MoPro*», *Journal of Applied Crystallography*, vol. 38 (1), pp. 38–54, URL http://dx.doi.org/10.1107/S0021889804025518. {Cited on pages xi and 12.}

[16] Johnson, E. R., Keinan, S., Mori-Sánchez, P., Contreras-García, J., Cohen, A. J. and Yang, W. (2010), «Revealing Noncovalent Interactions», *Journal of the American Chemical Society*, vol. 132 (18), pp. 6498–6506, URL http://pubs.acs.org/doi/abs/10.1021/ja100936w. {Cited on page 17.}

[17] Katan, C., Rabiller, P., Lecomte, C., Guezo, M., Oison, V. and Souhassou, M. (2003), «Numerical computation of critical properties and atomic basins from three-dimensional grid electron densities», *Journal of Applied Crystallography*, vol. 36 (1), pp. 65–73, URL http://dx.doi.org/10.1107/S0021889802018691. {Cited on page 26.}

[18] Kurki-Suonio, K. (1977), «IV. Symmetry and its Implications», *Israel Journal of Chemistry*, vol. 16 (2-3), pp. 115–123, URL http://dx.doi.org/10.1002/ijch.197700020. {Cited on page 53.}

[19] Kurki-Suonio, K. (1977), «VI. Charge Deformation Models», *Israel Journal of Chemistry*, vol. 16 (2-3), pp. 132–136, URL http://dx.doi.org/10.1002/ijch.197700022. {Cited on page 53.}

[20] Malcolm, N. O. J. and Popelier, P. L. A. (2003), «The full topology of the Laplacian of the electron density: scrutinising a physical basis for the VSEPR model», *Faraday Discuss.*, vol. 124, pp. 353–363, URL http://dx.doi.org/10.1039/B211650M. {Cited on page 21.}

[21] Mata, I., Molins, E. and Espinosa, E. (2007), «Zero-Flux Surfaces of the Electrostatic Potential: The Border of Influence Zones of Nucleophilic and Electrophilic Sites in Crystalline Environment», *The Journal of Physical Chemistry A*, vol. 111 (39), pp. 9859–9870, URL http://pubs.acs.org/doi/abs/10.1021/jp074032l, pMID: 17727276. {Cited on pages xi, 1, 3, 17, 24, and 26.}

[22] Mata, I., Molins, E., Alkorta, I. and Espinosa, E. (2007), «Topological Properties of the Electrostatic Potential in Weak and Moderate N···H Hydrogen Bonds», *The Journal of Physical Chemistry A*, vol. 111 (28), pp. 6425–6433, URL http://pubs.acs.org/doi/abs/10.1021/jp071924c, pMID: 17583329. {Cited on pages xi, 1, 3, and 17.}

[23] Matta, C. and Boyd, R., eds. (2007), *The Quantum Theory of Atoms in Molecules: From Solid State to DNA and Drug Design*, Wiley. {Cited on pages 1 and 3.}

[24] Murray, J. and Sen, K. (1996), *Molecular Electrostatic Potentials: Concepts and Applications*, Theoretical and Computational Chemistry, Elsevier Science. {Cited on page 24.}

[25] Netzel, J. and van Smaalen, S. (2009), «Topological properties of hydrogen bonds and covalent bonds from charge densities obtained by the maximum entropy method (MEM)», *Acta Crystallographica Section B*, vol. 65 (5), pp. 624–638, URL http://dx.doi.org/10.1107/S0108768109026767. {Cited on page 10.}

[26] Otero-de-la Roza, A., Johnson, E. R. and Luaña, V. (2014), «Critic2: A program for real-space analysis of quantum chemical interactions in solids», *Computer Physics Communications*, vol. 185 (3), pp. 1007 – 1018, URL http://www.sciencedirect.com/science/article/pii/S0010465513003718. {Cited on page xi.}

[27] Otero-de-la Roza, A. and Luaña, V. (2010), «Topological Characterization of the Electron Density Laplacian in Crystals. The

Case of the Group IV Elements», *Journal of Chemical Theory and Computation*, vol. 6 (12), pp. 3761–3779, URL http://pubs.acs.org/doi/abs/10.1021/ct100269e. {Cited on page 21.}

[28] Otero-de-la Roza, A., Blanco, M. A., Martín Pendás, A. and Luaña, V. (2009), «Critic: a new program for the topological analysis of solid-state electron densities», *Comput. Phys. Commun.*, vol. 180, pp. 157–166. {Cited on page xi.}

[29] Pathak, R. K. and Gadre, S. R. (1990), «Maximal and minimal characteristics of molecular electrostatic potentials», *The Journal of Chemical Physics*, vol. 93 (3), pp. 1770–1773, URL http://scitation.aip.org/content/aip/journal/jcp/93/3/10.1063/1.459703. {Cited on page 24.}

[30] Pendás, A. M., Francisco, E. and Costales, A. (2013), «Perspectives for quantum chemical topology in crystallography», *Physica Scripta*, vol. 87 (4), p. 048 106, URL http://stacks.iop.org/1402-4896/87/i=4/a=048106. {Cited on page 16.}

[31] Popelier, P. (2000), «On the full topology of the Laplacian of the electron density», *Coordination Chemistry Reviews*, vol. 197 (1), pp. 169–189, URL http://www.sciencedirect.com/science/article/pii/S0010854599001897. {Cited on page 17.}

[32] R. Daudel, M. E. S., R. F. W. Bader and Borrett, D. S. (1974), «The Electron Pair in Chemistry», *Can. J. Chem.*, vol. 52 (8), pp. 1310–1320, URL http://dx.doi.org/10.1139/v74-201. {Cited on page 17.}

[33] Santalo, N., Tarres, J., Espinosa, E., Llorca, J., Molins, E., Veciana, J., Rovira, C., Mays, M., Yang, S., Cowan, D., Garrigou-Lagrange, C., Amiell, J., Delhaes, P. and Canadell, E. (1993), «(BTDM-TTF)-TCNQ complex, a new organic metal», *Synthetic Metals*, vol. 56 (1), pp. 2050 – 2056, URL http://www.sciencedirect.com/science/article/pii/0379677993903713, proceedings of the International Conference on Science and Technology of Synthetic Metals (ICSM'92). {Cited on page xi.}

[34] Sanville, E., Kenny, S. D., Smith, R. and Henkelman, G. (2007), «Improved grid-based algorithm for Bader charge allocation», *Journal of Computational Chemistry*, vol. 28 (5), pp. 899–908, URL http://dx.doi.org/10.1002/jcc.20575. {Cited on pages 26 and 27.}

[35] Stalke, D., ed. (2012), *Electron Density and Chemical Bonding I: Experimental Charge Density Studies*, Electron Density and Chemical Bonding, Springer Berlin Heidelberg. {Cited on pages 1 and 3.}

[36] Stalke, D., ed. (2012), *Electron Density and Chemical Bonding II: Theoretical Charge Density Studies*, Electron Density and Chemical Bonding, Springer Berlin Heidelberg. {Cited on pages 1 and 3.}

[37] Stewart, R. F. (1969), «Generalized X-Ray Scattering Factors», *The Journal of Chemical Physics*, vol. 51 (10), pp. 4569–4577, URL http://scitation.aip.org/content/aip/journal/jcp/51/10/10.1063/1.1671828. {Cited on page 11.}

[38] Tang, W., Sanville, E. and Henkelman, G. (2009), «A grid-based Bader analysis algorithm without lattice bias», *Journal of Physics: Condensed Matter*, vol. 21 (8), p. 084 204, URL http://stacks.iop.org/0953-8984/21/i=8/a=084204. {Cited on pages 26 and 27.}

[39] Tsirelson, V. G., Avilov, A. S., Lepeshov, G. G., Kulygin, A. K., Stahn, J., Pietsch, U. and Spence, J. C. H. (2001), «Quantitative Analysis of the Electrostatic Potential in Rock-Salt Crystals Using Accurate Electron Diffraction Data», *The Journal of Physical Chemistry B*, vol. 105 (21), pp. 5068–5074, URL http://pubs.acs.org/doi/abs/10.1021/jp0015729. {Cited on pages 1, 3, 24, and 26.}

[40] Yu, M. and Trinkle, D. R. (2011), «Accurate and efficient algorithm for Bader charge integration», *The Journal of Chemical Physics*, vol. 134 (6), 064111, URL http://scitation.aip.org/content/aip/journal/jcp/134/6/10.1063/1.3553716. {Cited on pages 26 and 27.}

COLOPHON

This document was typeset in LaTeX using the typographical look-and-feel `arsclassica`. Most of the graphics in this thesis are generated using `VMD`, `Inkscape` and `pgf/tikz`. The bibliography is typeset using `natbib`.